CHAPTER V

RESULTS AND DISCUSSIONS

5.1 Characterization of chitosans

The charateristics of four chitosans selected for this study were presented in Table 5.1. HMW and MMW chitosans were commercially available and used without further purification. LMW and XLMW chitosans were produced from selectively enzymatic hydrolysis using chitinase and chitosanase, respectively.

To determine the degrees of deacetylation (DD), the correlation between degrees of acetylation (DA) and the ratio of absorbance A_{1320}/A_{1420} was used and expressed as follows [49]:

$$DA\ (\%) = 31.92(A_{1320}/A_{1420}) - 12.20 \qquad (5.1)$$

The relation correlates the reference band of structural unit that remained the same and the measured or characteristic band corresponding to the vibration of the structural unit which was eliminated after deacetylation process. The absorbance band at 1420 cm^{-1} was used as the reference band which represented C-H deformation and the characteristic band at 1320 cm^{-1} of C-N stretching was chosen to measure the extent of N-acetylation. Monal and coworkers [56] proved that the use of these bands to estimate the degrees of acetylation provided a better agreement in all ranges of degrees of acetylation from Nuclear Magnetic Resonance (NMR) technique than the use of 3450 cm^{-1} which represented the vibration of –OH groups as the reference band. The results on the degrees of deacetylation (DD) shown in Table 5.1 indicated that the degrees of deacetylation of all chitosan samples were in the range of 84 to 88%. Mao and coworkers [57] have suggested that chitosans with the degrees of deacetylation between 80 and 90% were suitable for uses in biomaterial applications.

To characterize the molecular weight of chitosan samples, two methods were used and the molecular weights calculated from two different basis, viscosity-averaged and weight-averaged, were compared. The most commonly used equation relating intrinsic viscosity, [η], with viscosity-averaged molecular weight, M_v, is Mark-Houwink equation; $[\eta] = KM_v^a$, where a and K are constants that are independent of M_v over a wide range of values. Recently, Terbojevich and coworkers [50], proposed the constants $K = 3.5\times10^{-3}$ and $a = 0.76$, found a good agreement in M_v values obtained by viscometry and absolute molecular weights from light scattering method. The constants $K = 3.5\times10^{-3}$ and $a = 0.76$ were used in this work and the viscosity-averaged molecular weights of chitosan samples were found to be in the range of 4.8k to 880k.

Interestingly, the viscosity-averaged molecular weights were much lower than weight-averaged molecular weights obtained by gel permeation chromatography (GPC). Since GPC technique required molecular weight standards having a certain range of molecular weight with a narrow molecular weight distribution, weight-averaged molecular weight highly depended on the standards used. Pullulans, which are highly flexible and uncharged polysaccharides, have been used as conventional standards in this study to determine the molecular weights of chitosans, which are more rigid and charged polysaccharides, resulting in vigorously overestimated molecular weights [58-60]. The stiffness of chitosan chains might result in a shorter time for the chains to move through the chromatography column although they have the same molecular weight as pullulans.

In conclusion, chitosans selected for this study had similar degrees of deacetylation, but they were markedly different in their molecular weights. All chitosan samples were used to study their influence of molecular weight on chemical, physical, and biological properties of collagen and chitosan scaffolds.

5.2 Chemical characterization of scaffolds

5.2.1 Fourier transform infrared (FT-IR) spectrophotometric analysis

The FT-IR spectra obtained from type I collagen was shown in Figure 5.1. In the spectrum of pure collagen, five characteristic absorption bands at the frequencies of 3439, 3300, 1660, 1550, and 1274 cm^{-1} were observed. Generally, amide I bands (1660 cm^{-1}) originate from C=O stretching vibrations coupled to N–H bending vibrations. The amide II bands (1550 cm^{-1}) arise from the N–H bending vibrations coupled to C–N stretching vibrations. The amide III (1274 cm^{-1}) is the combination peaks between N–H deformation and C–N stretching vibrations. The other two bands, arising from the stretching vibrations of free N–H group, of a medium to weak intensity, appear at 3324 cm^{-1} and the vibrations of hydroxyl group, –OH, appear at 3450 cm^{-1} [7]. For the spectrum of pure chitosan (Figure 5.1), it was well known that the characteristic absorption bands of chitosan appeared at six locations. The vibrations of hydroxyl and free amine groups appear at 3450 and 3324 cm^{-1}, respectively. The absorption bands at 1655, 1560, and 1381 cm^{-1} indicates C=O stretching, $–NH_2$ bending and C–O stretching of primary alcohol groups. The last one at 1152 cm^{-1} represented –C–O–C– glycosidic linkage between chitosan monomers [7, 45, 61]. The FT-IR spectra of XLMW, LMW, MMW, and HMW chitosans depicted the same characteristic absorption bands. This was the evidence that the selective enzymatic hydrolysis production of XLMW and LMW chitosan had an effect only on the molecular weight, not any significant changes in molecular level.

The FT-IR spectra of collagen/chitosan blends at various blending compositions, shown in Figure 5.2, depicted similar characteristic peaks of the parent molecules for all different molecular weight chitosans. For example, the intensity of amide I peak at 1658 cm^{-1} started to decrease slowly when increasing the proportion of chitosan. In addition, the interaction between collagen and chitosan could be still identified by amide I band and carboxylic bands presented in the range of 1600-1700 cm^{-1}. The small shifts could be observed on amide I band between the results from collagen/chitosan blends and that of pure collagen which might be simply attributed to

local modifications leading to small variations of the rotation and vibration frequencies. Moreover, the characteristic vibrations of a three-fold α-helix at 1637 cm^{-1} which was often attributed to a C—O group of imine type involved in hydrogen-bonding with water were still observed suggesting that the collagen molecules involved in collagen/chitosan blends were not denatured by the addition of chitosan [62]. On the other hand, the characteristic intense peak of chitosan, such as glycosidic linkages at 1152 cm^{-1}, appeared more clearly when the composition of chitosan in the blend was increased. For the spectra of chitosan dominate blends, the high proportion of chitosan was shown by an increase of the glycosidic linkage bands at 1152 cm^{-1} and by an decrease of the amide I band. To explain the contribution of collagen and chitosan in the blending solution, carboxylic groups, –COOH, of collagen were deprotonated to form carbonyl ions, $–COO^-$, while ammonium groups, $–NH_2$, of chitosan were protonated to form ammonium ions, $–NH_3^+$, at pH of blending solution less than 3.6. This caused solely electrostatic interaction between polyanionic collagen and polycationic chitosan [63]. This phenomena corresponded to the condition in the experiment, since the collagen/chitosan blending solutions were prepared using 0.5 M acetic acid (pH = 2.7). Moreover, the H-bonding interaction in collagen and chitosan complex could be occurred when pH of blending solution was approximately 5.8. At pH = 5.8, only a part of carboxylic and ammonium groups would be disassociated and formed electrostatic interaction. The rest of carboxylic and ammonium groups which could not be disassociated would form H-bonding interaction. As a result, H-bonding interaction of collagen and chitosan in the experiment could not be occurred. The contribution of collagen and chitosan in the experiment were, therefore, considered as purely electrostatic interaction without any chemical bonds. The results could be further confirmed by substraction of the FT-IR spectra of the collagen to the FT-IR spectra of the collagen/MMW chitosan (50/50) scaffold (line 50/50 in Figure 5.2c). The comparison between FT-IR spectra of chitosan obtained from substraction and pure chitosan was shown in Figure 5.3. The results revealed that there was no peak generated or disappeared after blending.

Figure 5.4 showed the peak analysis obtained from Peak Fit software (version 4.12) of amide I band of collagen/MMW chitosan (70/30) scaffold. One could also

notice the appearance of a new band at 1600 cm^{-1} attributed to the free amino band of chitosan and the total disappearance of the carboxylic band (1697 cm^{-1}) at the shoulder of amide I band. This implied that, under such conditions, the carboxylic groups of collagen which could not be accessible are now completely consumed. This evidence gave rise to chitosan content at 30%. It was interesting to note that this composition was close to the theoretical value of 28.5% calculated from purely electrostatic interaction between polyanionic collagen and polycationic chitosan. Purely electrostatic polyanion/polycation (PA/PC) complex in collagen and chitosan blends occurred when all carboxylic groups of collagen ionically interacted with ammonium groups of chitosan [63].

In addition, there was no obvious increase of the peak intensity at 1320 cm^{-1} representing the vibration of –CONH– bond which should be formed by condensation between –COOH of collagen and $–NH_2$ of chitosan after dehydrothermal treatment. This was because dehydrothermal treatment, a physical crosslink, possessed such a small crosslinking extent that could not be detected by FT-IR technique. This result was in good agreement with the work of Taravel and Domard [63].

In conclusion, the results indicated that the blends between collagen and different molecular weight chitosans had the same characteristic absorption bands without any appearance of new peaks and disappearance of the original bands of their parent molecules. Therefore, the FT-IR results suggested that there were only physical interactions between collagen molecules and chitosan molecules in the blends. Hence, they could exert their characteristics individually during in vitro culture studies. Thus the cells would avail the properties of both polymers.

5.2.2 Differential scanning calorimetric (DSC) analysis

The DSC curve of collagen/XLMW chitosan scaffolds with various blending compositions (Figure 5.5) showed a characteristic transition band attributed to the loss of bound water. It could also be observed that as the proportion of collagen increased the transition band shifted toward higher temperature since the water in collagen

polymer was more strongly bound than that in chitosan. The water transition temperatures of collagen/XLMW chitosan scaffolds were found at 113.0, 114.2, 111.7, 107.3, 105.3, 108.6, and 106.7°C for scaffolds containing 0, 10, 30, 50, 70, 90, and 100% of chitosan, respectively. Moreover, DSC analysis showed the decomposition temperature at 210.3 and 265.6°C for pure collagen and XLMW chitosan scaffolds, respectively. The DSC curves of collagen/XLMW chitosan scaffolds at blending ratio of 90/10 and 10/90 showed similar thermal characteristics to pure collagen and XLMW chitosan, respectively. The results were in good agreement with the work of Shanmugasundaram and coworkers [7].

5.3 Physical characterization of scaffolds

5.3.1 Compressive modulus

Compressive modulus of collagen/chitosan scaffolds was shown in Figure 5.6. In the case of pure components, the compressive modulus of pure collagen was approximately two times greater than those of pure HMW and MMW chitosans. Considering scaffolds of collagen with HMW chitosan, when increasing HMW chitosan contents up to 30%, the compressive modulus were increased. However, the further increase of chitosan composition more than 30% resulted in a decrease in the compressive modulus of the scaffolds. As the fraction of chitosan was as high as 90%, the compressive modulus was the same as that of pure chitosan scaffolds. But, for the scaffolds of collagen and the other chitosans (XLMW, LMW and MMW), the compressive modulus was started to decrease at the low concentration of chitosan and was further decreased when increasing the proportion of chitosan. This was similar to the previous work of Taravel and Domard [44] reported on the mechanical and biological properties of collagen and chitosan blends. They proposed that the presence of chitosan induced softening to collagen scaffolds.

It could be noticed that the molecular weight of chitosan had a significant effect on the compressive modulus of scaffolds. The scaffolds made from collagen and HMW chitosan had higher compressive modulus compared to those of lower

molecular weight ones. This may be attributed to the more ordered structure of the higher molecular weight chitosan. In addition, pure chitosan scaffolds with higher molecular weight had an advantage in compressive modulus since the longer polymeric chains accounted for better stiffness over the shorter ones [63]. On the other hand, the scaffolds composed of XLMW or LMW chitosans had lower compressive modulus and were more flexible relative to scaffolds containing MMW or HMW chitosans. Indeed, the compressive modulus of pure chitosan scaffolds was less than half of the values of pure collagen scaffolds. As a consequence, in contrast to what could be expected, the presence of approximately 30% of HMW chitosan in scaffolds could increase the compressive modulus of the scaffolds since at this blending composition collagen and HMW chitosan could theoretically form purely electrostatic system [62, 63]. The amino groups in chitosan chain were mainly incorporated in the formation of polyelectrolyte complex. Since the amino groups in chitosan chain were more available when the molecular weight of chitosan was higher, HMW chitosan could form polyelectrolyte complex better than other chitosan samples. This also confirmed that the chitosan chains really interacting in a collagen/chitosan polyelectrolyte complex which behaved like some polymer blends rather than three-dimensional networks. For this result, HMW chitosan could participate in the formation of collagen and chitosan complex better than XLMW, LMW, and MMW chitosans.

5.3.2 Swelling properties

The swelling ability of a scaffold is an important aspect to evaluate its property for skin tissue engineering. The swelling properties of scaffolds were determined by using phosphate buffer saline and the swelling ratios represented the amount of water uptake to the dry weight of scaffolds. The swelling characteristics of collagen/LMW, MMW, and HMW chitosan scaffolds at various blending compositions were shown in Figure 5.7. The scaffolds containing high collagen concentration revealed a rapid increase in water swelling and reached a high equilibrium swelling ratios, in the range of 6-8, within a few hours. The initial swelling rates of scaffolds having more chitosan content than 50% were slow and,

additionally, low equilibrium swelling ratios were observed comparing to scaffolds with high collagen concentrations. When increasing the proportion of chitosan to 70%, the equilibrium swelling ratios were slightly different from pure chitosan. At this blending composition, collagen/HMW chitosan scaffolds showed obviously low swelling ratio compared to scaffolds containing LMW or MMW chitosans. Since a large number of scaffolds were used to elucidate their dynamic swelling properties. For this reason, the dynamic swelling behavior of collagen/XLMW chitosan scaffolds was not performed because of a small amount of XLMW chitosan obtained. Furthermore, there was no significant difference in swelling behavior observed from blended scaffolds containing different molecular weight chitosans. Because collagen-based scaffolds revealed a rapid increase swelling ratios, the reliable swelling data were not obtained in the account of the very rapid swelling process. In order to verify the equilibrium swelling state, the scaffolds were immersed in 0.05 M phosphate buffer saline (pH 7.4) at 37°C for 24 h before the swelling measurements were carried out.

As shown in Figure 5.8, the equilibrium swelling ratios of collagen/chitosan scaffolds with different molecular weight of chitosan could be clearly distinguished into two groups. The first group of the blends containing chitosan less than 30% showed good swelling property same as that of pure collagen. The other group of which the swelling ratios were as low as that of pure chitosan was the blends having chitosan composition more than 30%. This was because they lost the gel-like structure after swollen in PBS. In addition, scaffolds composed of collagen and high molecular weight chitosan had lower swelling ability than that of low molecular weight chitosan, i.e. the equilibrium swelling ratio of scaffolds with 10% of XLMW chitosan was 31% higher than that of HMW chitosan. This might be the effect of low molecular weight chitosans that could be bound by surrounding water molecules more than the higher molecular weight ones. The collagen/chitosan scaffolds with the blending compositions of 100/0, 90/10, and 70/30 for all four molecular weights were selected to test the morphology and further biological characterization because of their excellent swelling ability. If the scaffolds were capably swollen, the pore sizes were allowed to in crease in diameter. The excellent swelling ratios could facilitate the cells

not only attach but also penetrate inside during *in vitro* culture studies. Those blends were considered to have high surface area and thus the cells can attach and grow in a three-dimensional fashion.

5.3.3 Morphology

Morphology of pure collagen scaffold revealed by SEM photographs illustrated in Figure 5.9, indicated the porous structure with three-dimensional interconnection throughout the scaffolds. Regardless of chitosan molecular weight, the interconnection of pores could still be observed when increasing the proportion of chitosan up to 30% (Figure 5.10-5.11). On the other words, no significant difference in morphology between collagen and collagen/chitosan scaffolds was noticed except a slight increase in pore sizes at high chitosan contents. This could be caused by the interaction of water in blended solution. When the collagen/chitosan solution was cooled in primary freezing step, water was separated from solutes as it changed to ice, creating more concentrated areas of solute. Since the results from DSC thermographs proved that water molecules could be more strongly bound by collagen than chitosan molecules, the generated ice crystals in the case of collagen dominate solution were found to have a smaller size than those of solution containing lower collagen contents. This caused a slightly enlarged pore size as increasing chitosan ratio in the blends.

Pore sizes of scaffolds fell in the range of 100-200 μm which was suitable for fibroblast infiltration reported by O' Brien and coworkers [2, 3]. For scaffolds at blending composition of 90/10 (collagen/chitosan) as shown in Figure 5.10, the morphology was seem to have more ordered structure when the molecular weight of chitosan became higher. The results could also be observed from either blending composition of 70/30 (Figure 5.11) or pure chitosan scaffolds (Figure 5.12). There was markedly different in the morphology of scaffolds fabricated from various molecular weight chitosans. The more ordered structure could be obtained from HMW chitosan.

5.4 Biological characterization of scaffolds

5.4.1 Biodegradation

The specific degradation by lysozyme of collagen and different molecular weight chitosans can be beneficial in tissue engineering application since lysozyme is presented in certain human body fluids [55, 65]. In addition, lysozyme was reported to be synthesized during active phagocytosis after injury [66]. Thus lysozyme, released from phagocytic cells including macrophages, will be available for the degradation of dermal regeneration templates based on collagen and chitosan. To evaluate the biodegradation of the scaffolds, samples were incubated in lysozyme containing phosphate buffer saline (pH 7.4). The biodegradation of scaffolds has already been studied [44, 46, 67-69]. However, most of the studies were performed under accelerated conditions using low pH for optimum lysozyme activity as well as high enzyme concentrations. To mimic human serum condition, long-term *in vitro* studies using physiological pH and enzyme concentration as described in section 4.3.6.1 have rarely been studied. To distinguish between enzymatic degradation and sample dissolution, the dissolution of the two components either collagen or chitosan in scaffolds could be neglected. Since it was well known that both collagen and chitosan were insoluble in water. Therefore, the enzymatic degradation of these scaffolds was mainly considered.

The biodegradation results were depicted in Figure 5.13. Collagen scaffolds incubated in lysozyme had the highest weight reduction and were completely degraded after three weeks. However, addition of chitosan, especially HMW chitosan, reduced degradation of scaffolds in lysozyme solution. This suggested that the physical interaction between collagen and chitosan possessed more steric hindrance effect to specific cleavage sites of lysozyme than that of the pure collagen [44]. It is well known that, in human serum, either collagen or chitosan are mainly depolymerized by lysozyme [67]. This was because lysozyme is a mucolytic enzyme with antibiotic properties and a typical globular protein, incorporating many secondary structure consisting of fourteen turns, an assortment of large and small α-

helices, a few short of β-sheets, and four disulfide bonds. In addition, lysozyme indicated a single cleavage site between Typ-108 and Val-109 of N-terminal of protein fragments. Type I collagen, which is the helical protein, generally appeared the amorphous region where lysozyme could penetrate and depolymerize at N-(1-phenlyalanine)-4-(1-pyrene)butyramide(Py-Phe) [70]. For chitosan, the general mechanism is that lysozyme degraded chitosan, the heteropolysaccharides, by hydrolyzing the glycosidic bonds presented in the chemical structure as described in section 5.2.1. Lysozyme contains a hexameric binding site [68], and hexasaccharide sequences containing 3-4 or more acetylated units contributing mainly to the initial degradation rate of chitosan [69].

When the proportion of chitosan was increased to 30%, the remained weights were sustained after 3 weeks at 21%, 48%, 61%, and 71% for XLMW, LMW, MMW, and HMW chitosans, respectively. For the scaffolds with 50% chitosan, the remained weights were approximately 26%, 74%, 79%, and 82% for XLMW, LMW, MMW, and HMW chitosans, respectively. At the end of 4 weeks, the net weight of collagen/chitosan scaffolds in lysozyme were increased as increasing the fraction of chitosan and it was true for four different molecular weights of chitosan. The pattern of degradation of collagen/chitosan scaffolds found in this study could be explained by following mechanism of enzymatic degradation. After a high initial mass loss, the degradation rate of the samples generally slowed down for scaffolds having higher chitosan content, i.e. 30% and 50% of either MMW or HMW chitosans, as shown in Figure 5.13c-5.13d. Probably no further degradation could occur in scaffolds containing either MMW or HMW chitosan at 30% and 50% after 3 weeks due to the lack of acetyl groups, necessary for lysozyme binding. The lack of consecutive N-acetaminoglucosamine residues was also responsible for the slow degradation of scaffolds. However, scaffolds having XLMW or LMW chitosans showed the fast decreasing degradation rate although the chitosan contents were as high as 30% relative to those scaffolds with MMW or HMW chitosans. This might be due to HMW chitosans having more glycosidic linkage which served as specific cleavage sites for lysozyme than that of the LMW chitosans. For this reason, HMW chitosan could resist to lysozyme degradation better than the other chitosans. On the other

hand, the chains of XLMW and LMW chitosans were much shorter resulting in a less resistance to lysozlyme degradation than the case of scaffolds with MMW or HMW chitosans.

Moreover, another aspect to explain the degradation of collagen/chitosan scaffolds was a difference in hydrophobicity and crystallinity of chitosans presented in scaffolds. It could be noticed that biodegradation increased rapidly at the onset of hydrolysis, but the rate of increase reduces as hydrolysis proceeded (see Figure 5.13). Several reports [71, 72] have suggested that such reduction can be attributed to several factors such as inhibition of enzyme action by the accumulated products, partial enzyme inactivation. However, these conclusions did not correspond to the experiments performed in this study since the lysozyme solution was freshly changed everyday during degradation test to mimic the blood circulation in physiological condition. The most reasonable explanation is the decreasing in enzymatic accessibility as the proportion of crystalline zones in the residual substrate increases. This is in a good agreement with the results that scaffolds containing XLMW or LMW chitosans can be digested faster than those consisting of MMW or HMW chitosans since the MMW or HMW chitosans can form more stable crystalline region than lower molecular weight chitosans.

Because of low crystallinity and relatively weak intermolecular forces, low molecular weight chitosan proved to be more susceptible to lysozyme than high molecular weight ones. This can be evidenced by the degradation curves of scaffolds with MMW or HMW chitosans which showed the plateau region after 3 weeks when the proportions of chitosan were as high as 30%. The amorphous portion of chitosan was hydrolyzed more quickly than the crystalline region. Moreover, the degradation rate of scaffolds composed of 30% XLMW chitosan was appreciably promising to the biodegradation time required for healing acute skin wounds which was about 25 days [73]. A more rapid degradation rate would reduce the scaffold within a few days to the liquid state, rendering its ineffectiveness as a skin substitutes. On the other hand, a scaffold that degraded minimally within 3-4 weeks would hinder the wound healing

process [73]. The results proved that the addition of chitosan could prolong the degradability of scaffolds which was the vital characteristic for skin substitutes.

5.4.2 L929 and Detroit 551 cell adhesion and proliferation tests

The extracellular matrix is composed of glycosaminoglycan and collagen. This matrix controls the proliferation of cells for maintenance of hemostatis and regeneration of damaged tissues. An artificial matrix, with controlling functions like those of the normal extracellular matrix, is important for the reconstruction of complex organs, which is the aim of tissue engineering and regenerative medicine. Cell adhesion and proliferation are crucial for a scaffold to support and guide tissue regeneration. L929 cells were seeded onto substrates and cultured in DMEM medium. Figure 5.14 showed the initial cell adhesion at 5 h after seeding. The results showed no significant difference between collagen, collagen/chitosan, and chitosan scaffolds. Moreover, the results elucidated that molecular weights of chitosan did not have a dramatic effect on initial cell adhesion.

Figure 5.15a-5.15c represented the results of the mitochondrial activity (MTT) assay for cell proliferation performed in FBS-supplemented medium at 5, 24, and 72 h after seeding. L929 cells were seeded on the collagen (control), collagen/chitosan, and chitosan scaffolds to compare their cell behavior. The average percentage of cell viability of proliferation was reported from six different assays (n = 6). As what would be expected, the results indicated that there were no significant differences between the cell adhesion on whether collagen, collagen/chitosan, and chitosan scaffolds ($P<0.05$) at 5 h. The similar initial cell behavior could be observed for all scaffolds regardless of the blending compositions and molecular weight of chitosan. For scaffolds of pure LMW, MMW, and HMW chitosans, it should be pointed out that L929 cells did not proliferate on these pure chitosan scaffolds in this study. It was indicated by the very small increase in cell viability obtained after 72 h of seeding. This might be due to the inhibition of fibroblast migration by very high affinity between positively charged chitosan and negatively charged surface of cells. For pure collagen scaffolds, the percentage of cell viability at 72 h after cell seeding was about

1.6 folds of 5 h after seeding. The scaffolds with 30% chitosan expressed the most significant increase in relative cell viability among the three different molecular weight of chitosans. At this fixed chitosan composition, scaffolds blended with LMW chitosan showed the highest increase in relative cell viability at 72 h with significant difference ($p<0.05$). The results revealed that the incorporation of chitosan into collagen scaffolds at this blending composition could progressively promote L929 cell proliferation. In addition, for scaffolds containing 30% of LMW chitosan, the percentage of cell viability was significantly increased, $P<0.01$, relative to control. The results evidenced that low molecular weight chitosans can better accelerate and promote L929 cell proliferation than high molecular weight ones.

The effects of chitosan on the cell behavior might be explained as follows. Collagen, when crosslinked by DHT, some specific cell binding amino acids which interact with cell surface integrin adhesion receptors might be consumed [5]. Addition of chitosan may provide much more amino groups for cell adhesion and proliferation due to the affinity between positively charged ammonium groups at physiological pH of chitosan and negatively charged cell membrane surfaces [57, 74]. The influence of different molecular weight on the cell activity may be explained as the synergistic interaction between LMW chitosan and secreted proteins from cells which can maintain the optimal environment for cell growth. In case of pure chitosan, the growth of L929 cells might be inhibited by the extremely high affinity of cells with chitosan. Consequently, the addition of chitosan could enhance the proliferation of L929 on the collagen/chitosan scaffolds.

To confirm the stimulation of LMW chitosan on L929 mouse fibroblast proliferation, the effects of serum component were investigated. Cells were seeded onto scaffolds with mimic conditions except the presence of serum in medium. The results, depicted in Figure 5.16a-5.16c, showed similar characteristic of cell behavior with a slight difference in the relative cell viability since cell response was delayed with the absence of serum in medium, Scaffolds containing 70% of collagen and 30% of LMW chitosan still predominantly stimulated L929 proliferation. The results confirmed that 30% of LMW chitosan presented in collagen-based scaffolds had the

better synergistic effects with growth factors or some secreted protein from cells. Our cell proliferation results corresponded with the work on the effect of chitin and chitosan on the proliferation of human dermal fibroblasts *in vitro* reported by Howling and coworkers [8]. The proliferation test was observed in human dermal fibroblast cultured for 3 days in medium containing soluble fraction of chitosan. They found that low molecular weight chitosan (M_{av} = 13,000 measured by intrinsic viscosity and light scattering method) displayed higher proliferation activity than high molecular weight chitosan (M_{av} = 263,800). The maximal stimulation was observed in fibroblasts cultured in medium containing 5 μg/mg of low molecular weight chitosan. The mechanism by which LMW chitosan strongly stimulated L929 proliferation could be explained as LMW chitosan might bind serum components such as growth factors and either protect them from enzymatic degradation or present them to cells in an activated from. Bound growth factors could be slowly released by the action of lysozyme on chitosan, supplying the cells with a sustained level of mitogenic signals [75-77].

Since the scaffolds fabricated in this work were aimed to be used in skin tissue engineering, the proliferation test was further evaluated using Detroit 551 human dermal fibroblasts. This was because Detroit 551 cells, finite-passage cell line, expressed the better representative *in vitro* for model of dermal wound healing than L929 cells (continuous cell line). In the further study, XLMW chitosan with M_v = 4.8k was taken into account for Detroit 551 cell proliferation test. Detroit 551 cells were cultured on various matrices with the same conditions as L929 cells. Figure 5.17 showed the results of MTT assay for initial cell adhesion cultured in FBS-supplemented medium at 5 h after seeding. The results were similar to the case of L929 cells. Neither molecular weight nor blending composition significantly affected the initial cell adhesion of Detroit 551 cells. Figure 5.18a – 5.18c indicated the results of Detroit 551 cell proliferation cultured in FBS-supplemented medium at 5, 24, and 72 h after cell seeding. The percentages of relative cell viability were lower than those of L929 cell proliferation. This was because Detroit 551 cells had lower activity than L929 cells. After 5 h, there was no significant difference among pure chitosan scaffolds. Considering scaffolds with 30% chitosan, the percentages of relative cell

viability of scaffolds containing XLMW or LMW chitosans were slightly greater than those of scaffolds containing MMW or HMW chitosans at 24 h after seeding. At 72 h after seeding, it was remarkably noticed that scaffolds composed of 30% XLMW illustrated the highest relative cell viability, indicating an excellent stimulation on Detroit 551 cell proliferation. This proved our hypothesis that chitosan with a very low molecular weight could vigorously stimulate cell activity. Interestingly, relative cell viability at 72 h of scaffolds containing 10% XLMW chitosan was significantly increased compared to the other chitosan and pure collagen scaffolds. The results might imply that there could be a shift in the effective concentration of chitosan toward the lower concentration end for maximal stimulation when the molecular weight of chitosan was very low.

In order to verify the affinity of human dermal fibroblasts on the scaffolds, collagen, collagen/XLMW chitosan (70/30), and XLMW chitosan scaffolds after culture periods of 72 h were selected to observe cell morphology. Figure 5.19 exhibited the affinity and distribution of fibroblasts on scaffolds after culture periods of 72 h. The figures showed cells as white circular spot proliferated and distributed well in collagen and collagen/XLMW chitosan scaffolds, whereas cell proliferation was inhibited in XLMW chitosan scaffold. For pure XLMW chitosan scaffold, the cells showed signs of increased cellular marking and rounding-off of some cells leading to death. Furthermore, cells on XLMW chitosan scaffold were found to have a reduction in cell size. This was because they had very high affinity to pure chitosan, resulting in the inhibition of cell proliferation. This was in a good agreement with the results of relative cell viability reported in section 5.4.2. The results confirmed that scaffolds fabricated from XLMW chitosan and collagen were more biological active than pure collagen or chitosan, and possibly had more potential as wound healing agents or dressing materials.

5.4.3 Detroit 551 cell spreading area observation

Figure 5.20-5.25 showed the SEM micrographs of spreading behavior of Detroit 551 human dermal fibroblasts on the collagen, collagen/XLMW chitosan, and XLMW chitosan scaffolds. Collagen/XLMW chitosan scaffold with blending composition of 70/30 was selected to observe its interaction with Detroit 551 cells since it could promote the highest cell proliferation among all scaffolds. Pure collagen and XLMW chitosan scaffolds were also selected since they served as positive and negative controls, respectively. To access the cell spreading area on these materials, scaffolds were serially sectioned as described in section 4.3.6.3. Figure 5.20 -5.22 showed the SEM micrographs of cross-sectional planes of scaffolds. The micrographs demonstrated that fibroblasts cultured on these scaffolds remained viable and also maintained spindle morphology after 72 h. For pure collagen scaffolds, Detroit 551 cells could penetrate through the thickness of scaffolds (Figure 5.20). Cells could be observed on the scaffold from cell seeding side (Figure 5.20a) toward bottom side (Figure 5.20d). The similar observation can be found in the case of scaffolds containing 30% XLMW chitosan (Figure 5.21). For pure XLMW chitosan scaffolds, Detroit 551 could migrate approximately 20% of scaffold thickness (Figure 5.22).

Considering the SEM micrographs of the horizontal planes of scaffolds shown in Figure 5.23-5.25, the homogeneous distribution of cells was also observed in both collagen and collagen/XLMW chitosan scaffolds which corresponded to that seen in cross-sectional plane. For pure XLMW chitosan scaffold, human dermal fibroblasts could migrate only about 30% of scaffold radius from the edge (Figure 5.25). Cells were found only on the edge of the scaffold (Figure 5.25a), but they were disappeared when looked toward the center of the scaffold (Figure 5.25b-5.25d). In addition, the fibroblast spreading area on collagen/XLMW chitosan scaffold was comparable to that on pure collagen scaffold, and much higher than that on pure XLMW chitosan scaffold. The ability of chitosan to support cell survival could be attributed to its chemical properties. In other words, the resemblance of chitosan to the components of proteoglycans might be conductive to cell adhesion and proliferation. However, there were not many fibroblasts on the pure XLMW chitosan scaffold. The growth of

fibroblasts might be inhibited by the extremely high affinity of fibroblasts with chitosan. This corresponded to the results of cell proliferation reported in section 5.4.2. The activity of living fibroblasts was found to be relatively higher when seeded on collagen/XLMW chitosan scaffold as compared to pure collagen scaffold. The results ensured that collagen/XLMW chitosan scaffolds looked very promising to be a biocompatible material for dermal regeneration.

Table 5.1 Characteristics of chitosans used in this study.

Chitosan	DD[a](%)	$[\eta]^b$(ml/g)	M_v[c]	M_w[d](Da)
XLMW	86.13	22.1	4.8k	49k
LMW	87.91	176.1	74k	180k
MMW	84.43	531.2	320k	460k
HMW	85.83	1,170.8	880k	1,450k

[a] Degree of deacetylation was determined by FT-IR spectroscopy.

[b] Intrinsic viscosity was measured by Ubbelohde viscometer.

[c] Viscosity-averaged molecular weight was calculated from the intrinsic viscosity using the classical Mark-Houwink equation $[\eta] = KM_v^a$, where the constants $K = 3.5\times10^{-3}$ and $a = 0.76$ [52].

[d] Weight-averaged molecular weight was determined from gel permeation chromatography technique.

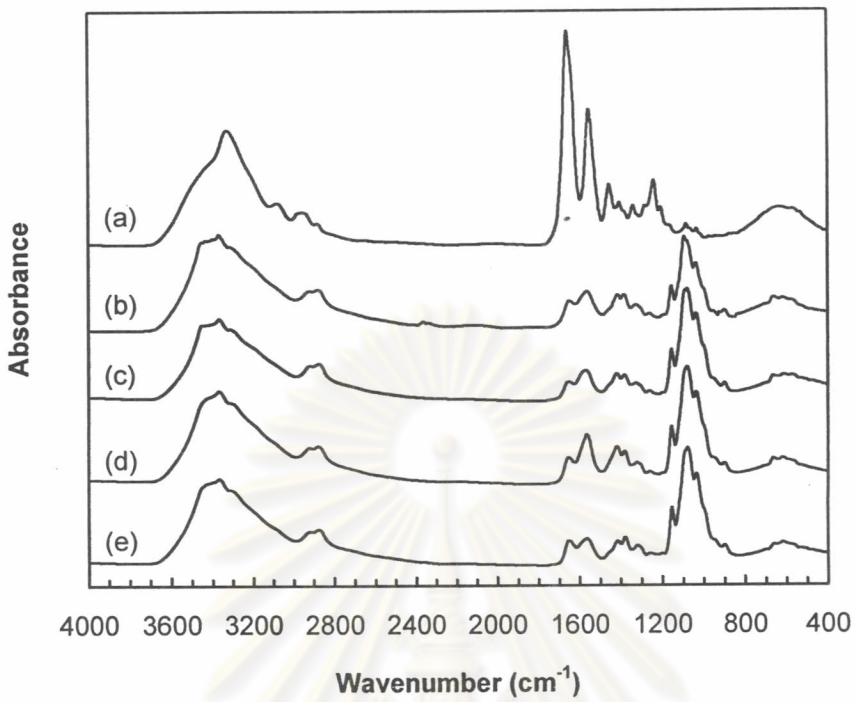

Figure 5.1 FT-IR spectra of pure components: (a) type I collagen, (b) XLMW, (c) LMW, (d) MMW, and (e) HMW chitosans.

(a)

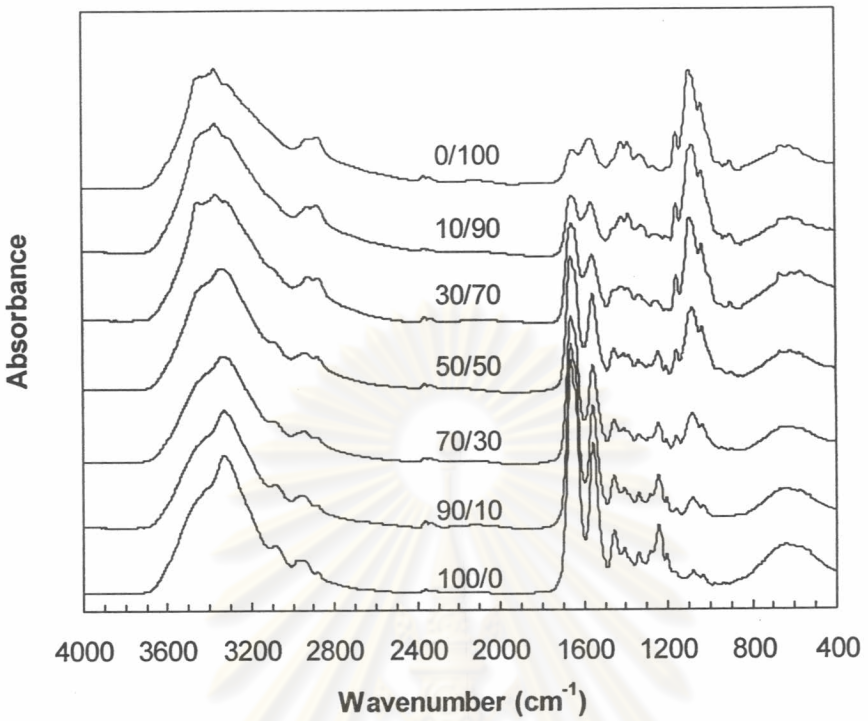
0/100
10/90
30/70
50/50
70/30
90/10
100/0
Absorbance
4000 3600 3200 2800 2400 2000 1600 1200 800 400
Wavenumber (cm-1)

(b)

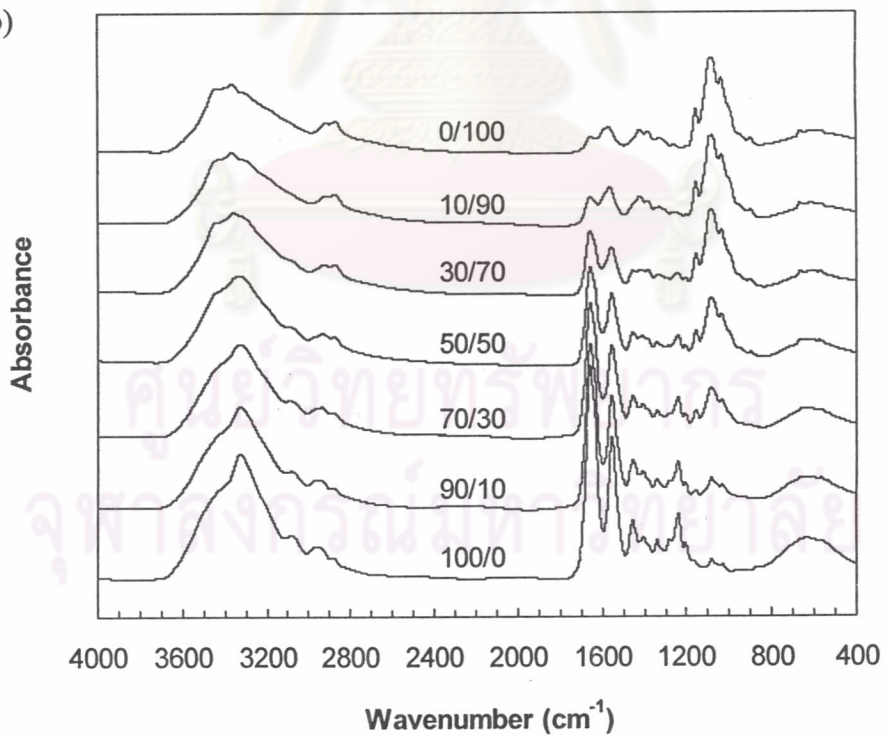
0/100
10/90
30/70
50/50
70/30
90/10
100/0
Absorbance
4000 3600 3200 2800 2400 2000 1600 1200 800 400
Wavenumber (cm-1)

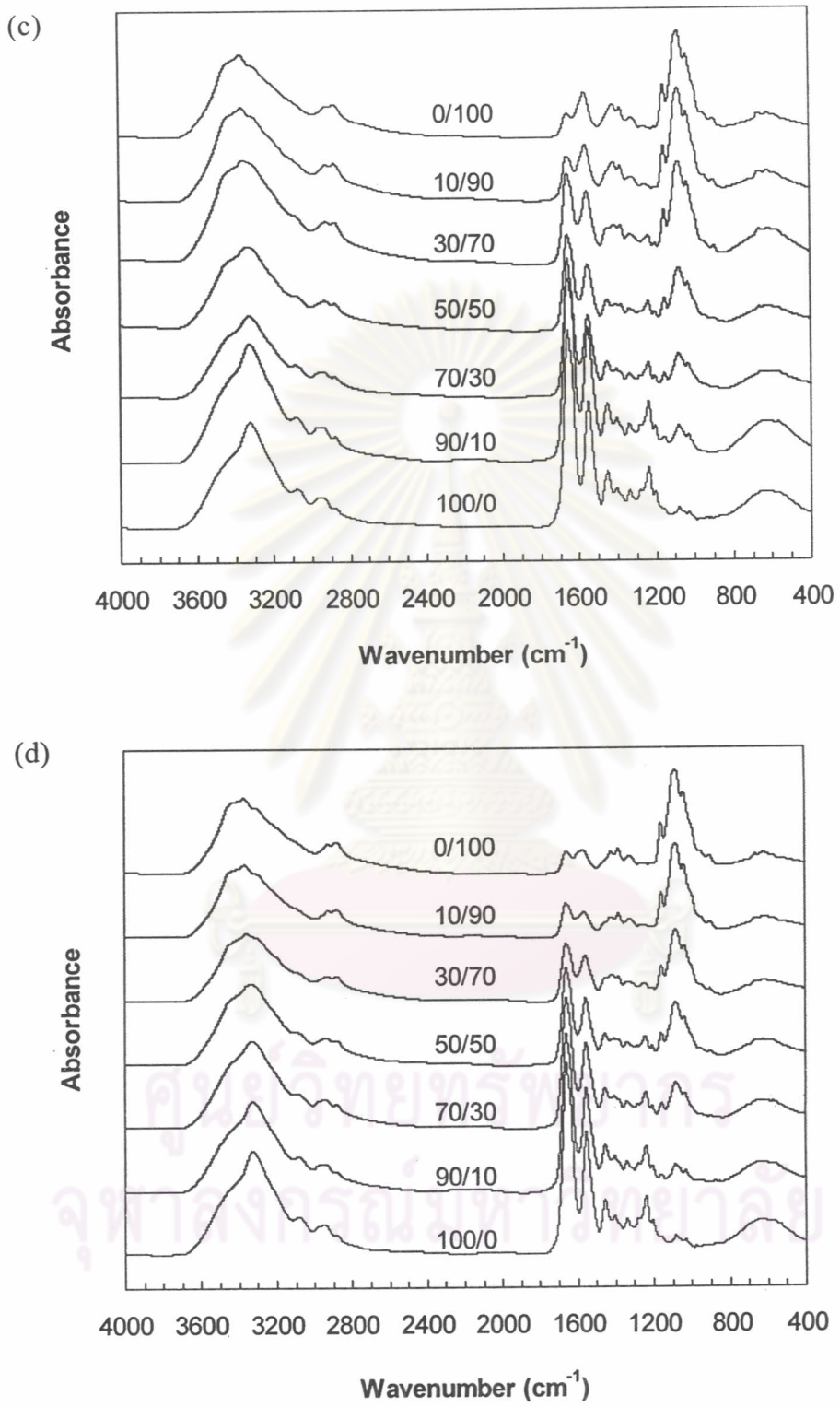

Figure 5.2 FT-IR spectra of various blends between type I collagen and (a) XLMW, (b) LMW, (c) MMW, and (d) and HMW chitosans (collagen to chitosan ratios were indicated for each spectrum).

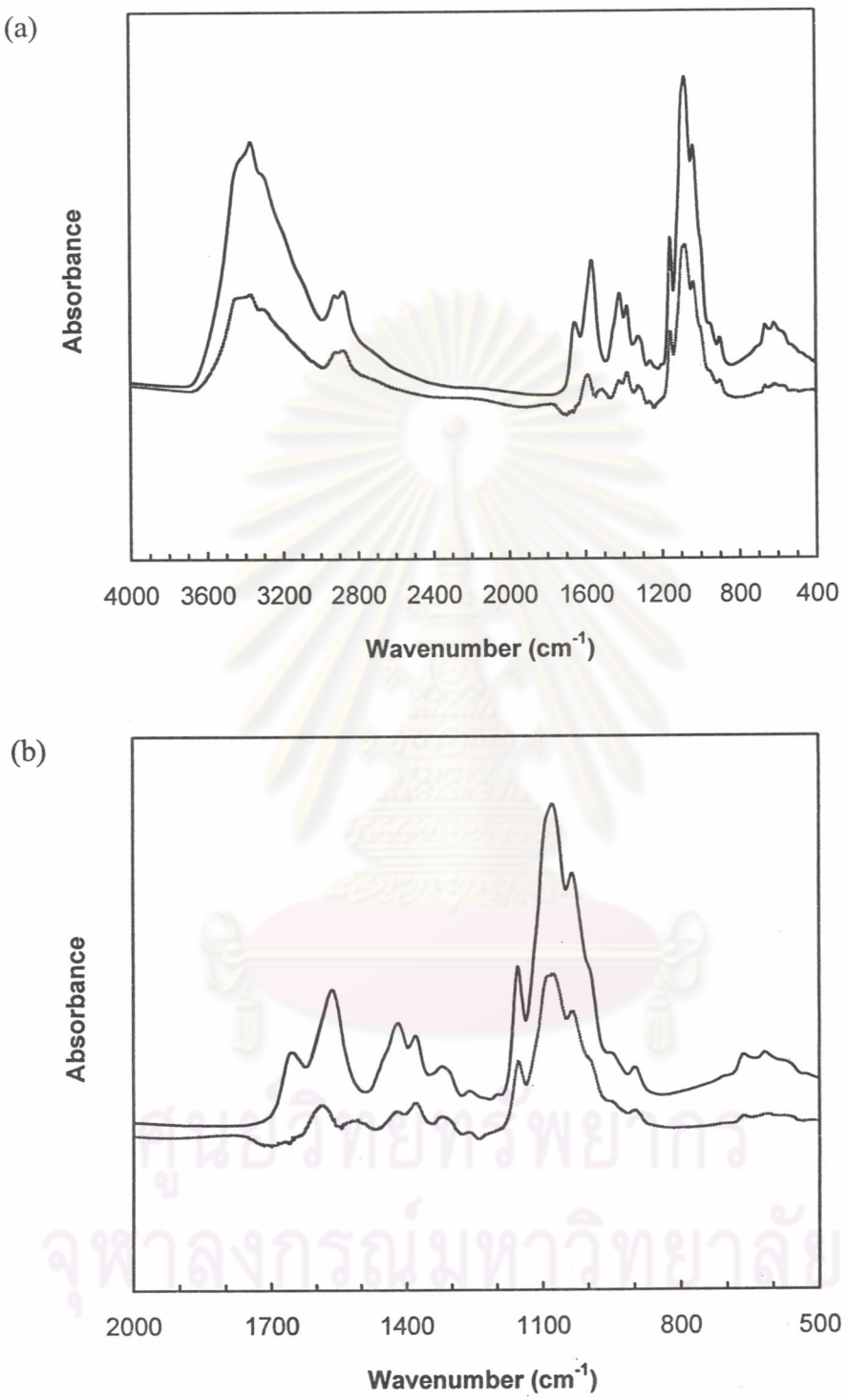

Figure 5.3 FT-IR spectra obtained after substraction of the normalized collagen spectra to the collagen/MMW chitosan (50/50) spectra (dark line) and FT-IR spectra of pure MMW chitosan (dash line): (a) 4000-400 cm^{-1} and (b) 2000-500 cm^{-1}

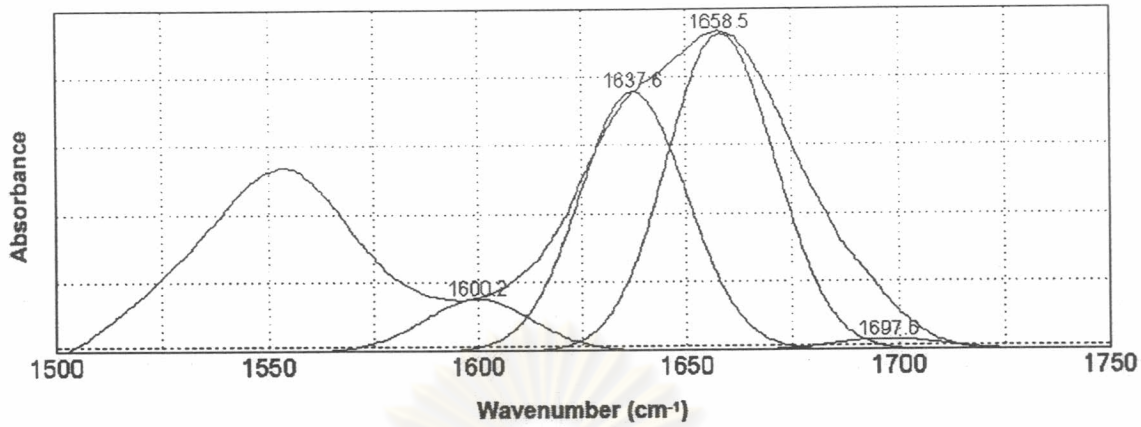

Figure 5.4 Peak analysis obtained from Peak Fit software (version 4.12) of amide I band of collagen/MMW chitosan (70/30) scaffolds.

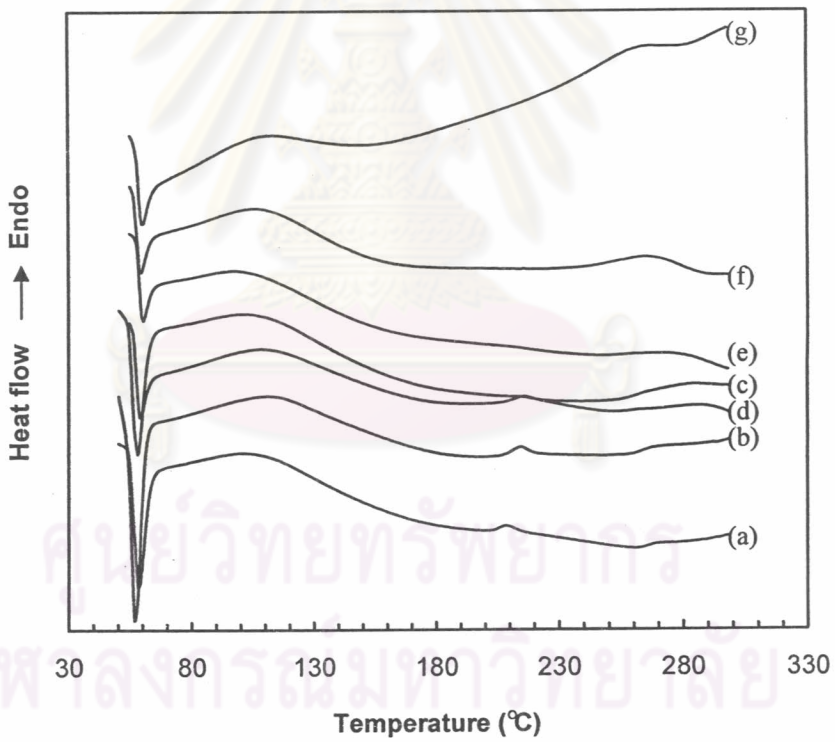

Figure 5.5 DSC thermographs of collagen/XLMW chitosan scaffolds carried out at the heating rate of 20°C/min. Different blending compositions as follows: (a) 100/0, (b) 90/10, (c) 70/30, (d) 50/50, (e) 30/70, (f) 10/90, and (g) 0/100.

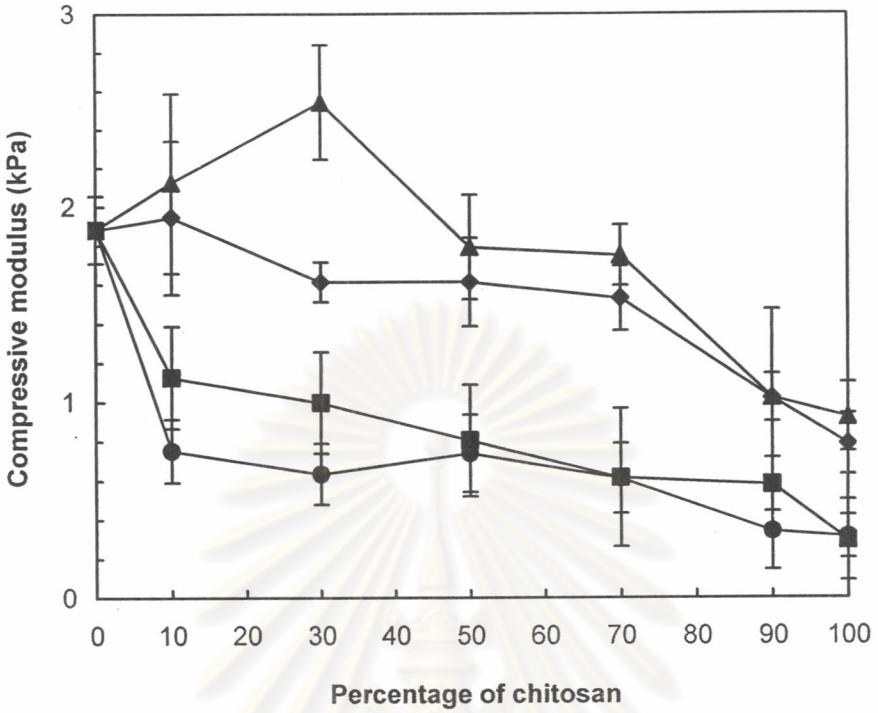

Figure 5.6 Compressive modulus of scaffolds of collagen blended with (●) XLMW, (■) LMW, (♦) MMW, and (▲) HMW chitosans.

(a)

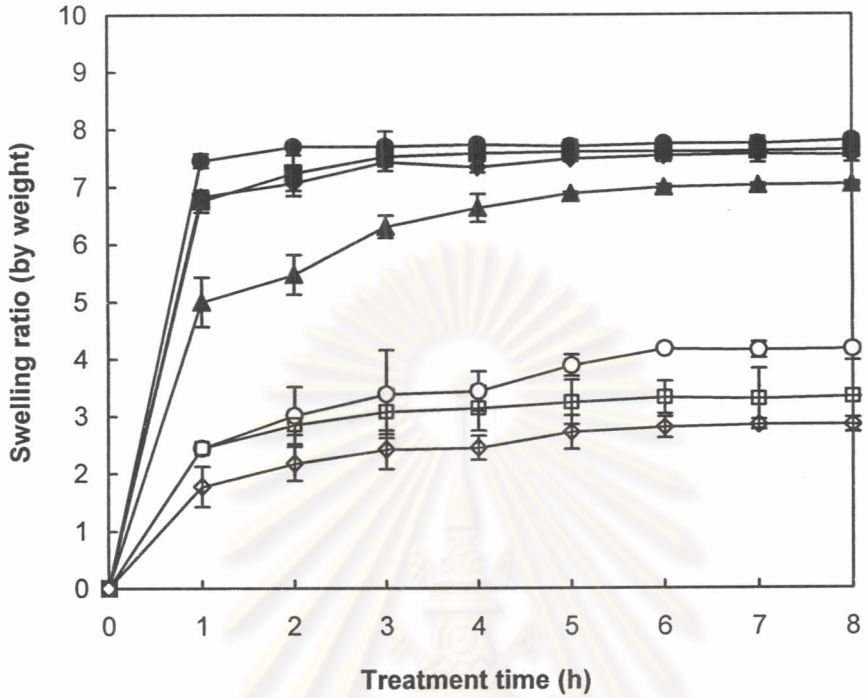
Swelling ratio (by weight)
Treatment time (h)
0
1
2
3
4
5
6
7
8
9
10

(b)

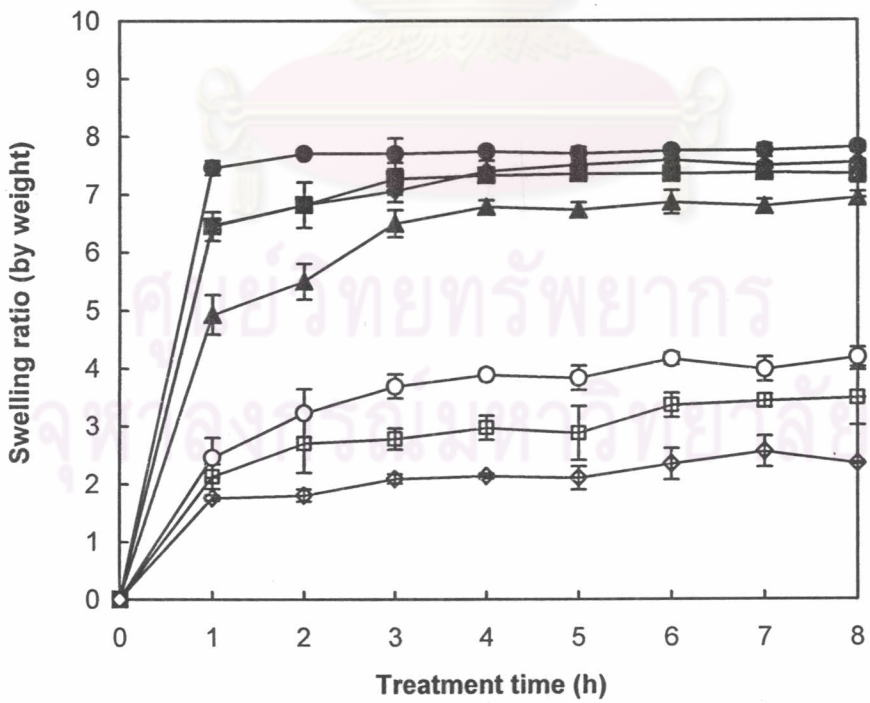
Swelling ratio (by weight)
Treatment time (h)
0
1
2
3
4
5
6
7
8
9
10

(c)

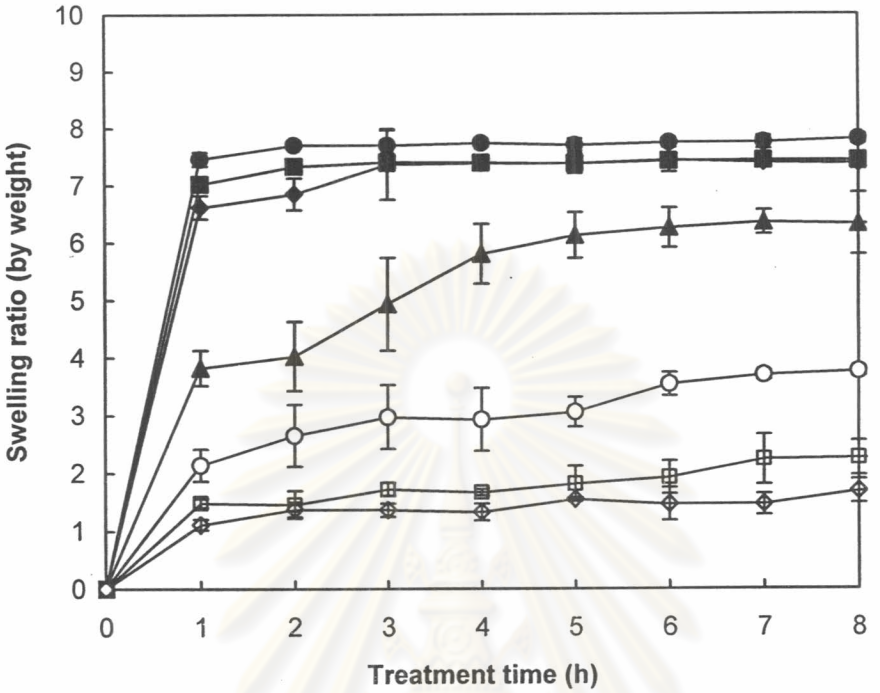

Figure 5.7 Swelling kinetics of various blending compositions of scaffolds between type I collagen and (a) LMW, (b) MMW, and (c) HMW chitosans: (●) 100/0, (■) 90/10, (♦) 70/30, (▲) 50/50, (○) 30/70, (□) 10/90, and (◊) 0/100 (ratios of collagen to chitosan).

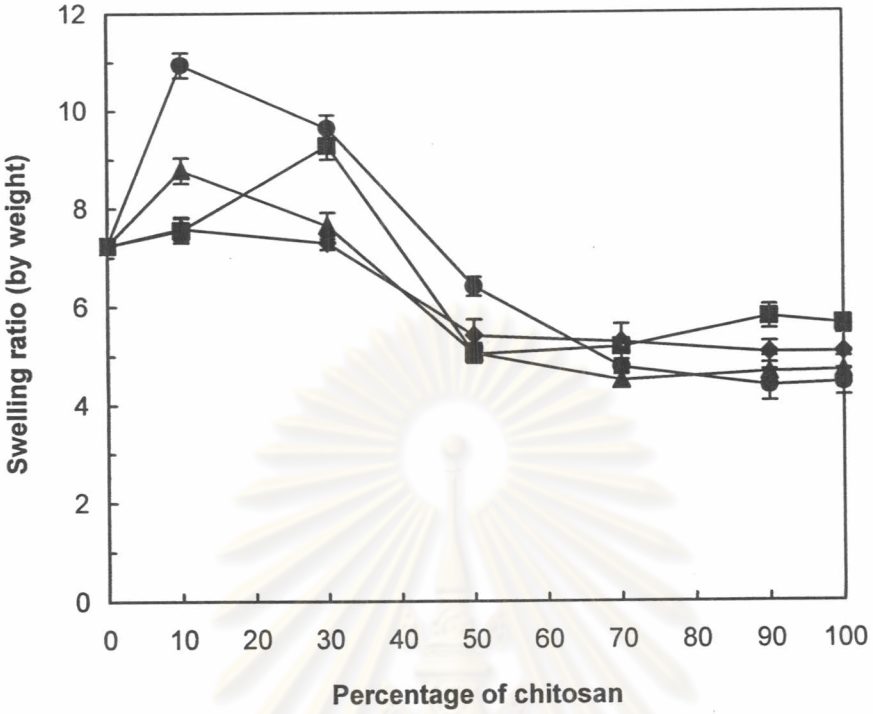

Figure 5.8 Equilibrium swelling ratios of collagen/chitosan scaffolds with different molecular weights: (●) XLMW, (■) LMW, (♦) MMW, and (▲) HMW chitosans.

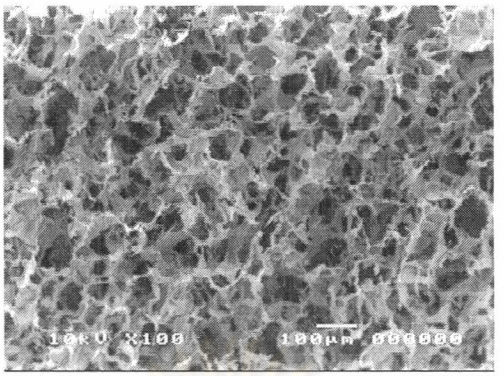

Figure 5.9 SEM micrograph of collagen scaffolds.

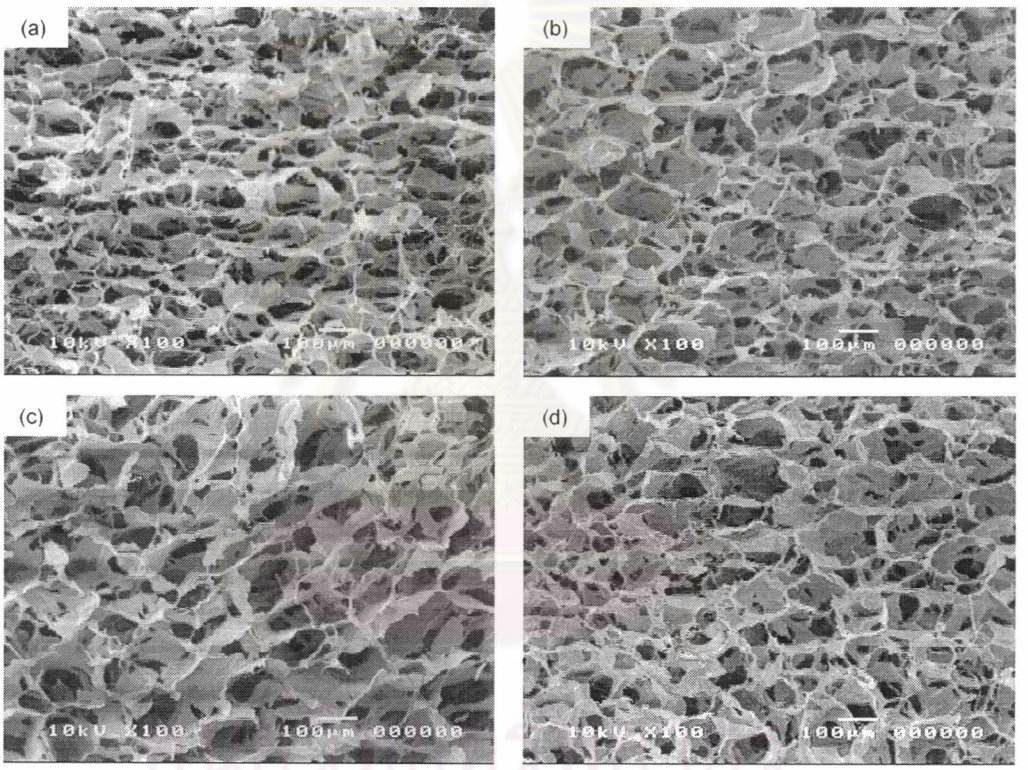

Figure 5.10 SEM micrographs of collagen/chitosan scaffolds at blending compositon of 90/10: collagen blended with (a) XLMW, (b) LMW, (c) MMW, and (d) HMW chitosans.

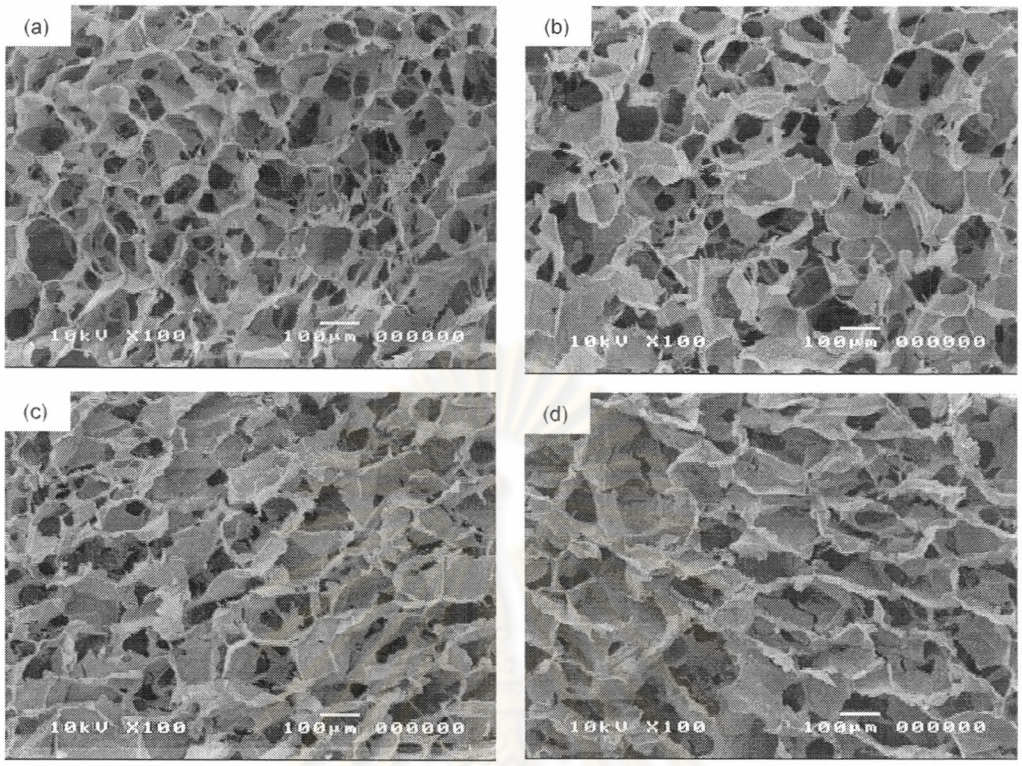

Figure 5.11 SEM micrographs of collagen/chitosan scaffolds at blending compositon of 70/30: collagen blended with (a) XLMW, (b) LMW, (c) MMW, and (d) HMW chitosans.

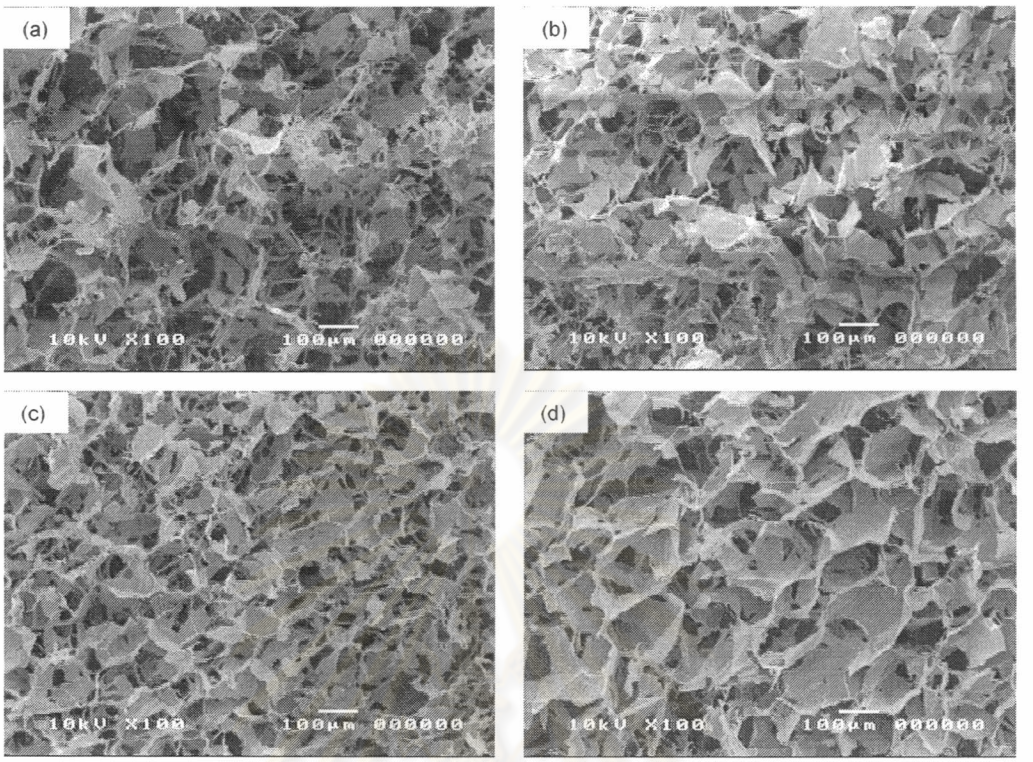

Figure 5.12 SEM micrographs of chitosan scaffolds: (a) XLMW, (b) LMW, (c) MMW, and (d) HMW chitosans.

(a)

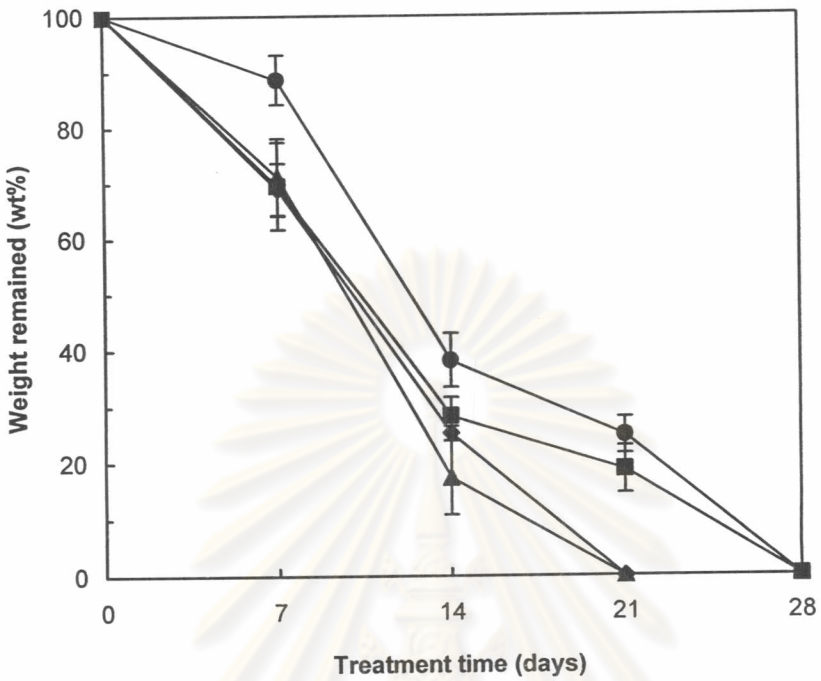

(b)

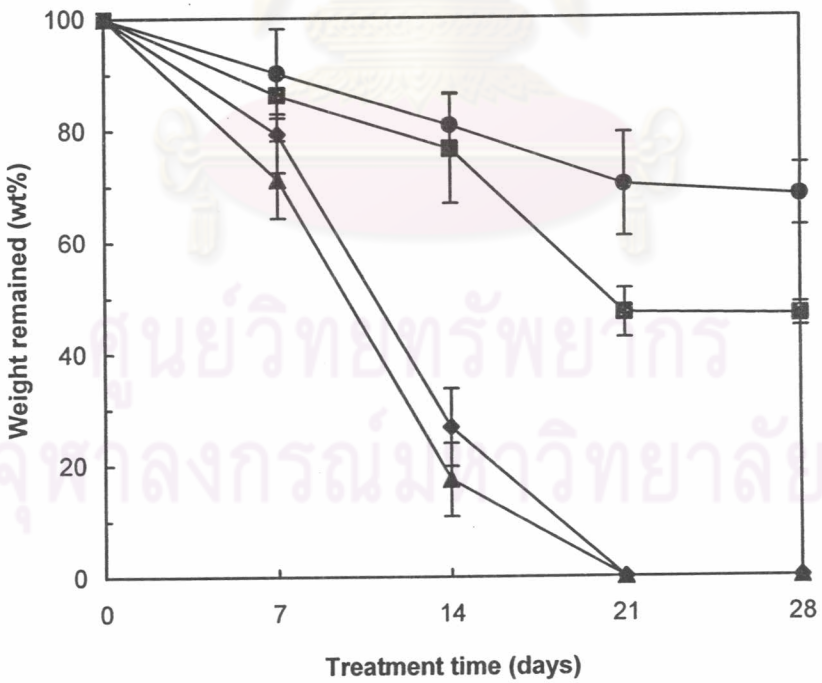

(c)

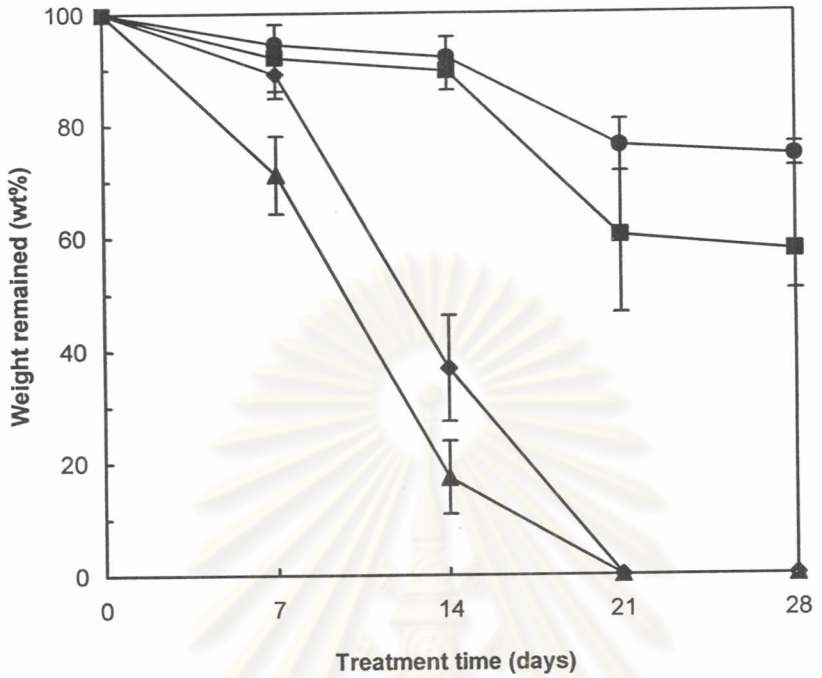

(d)

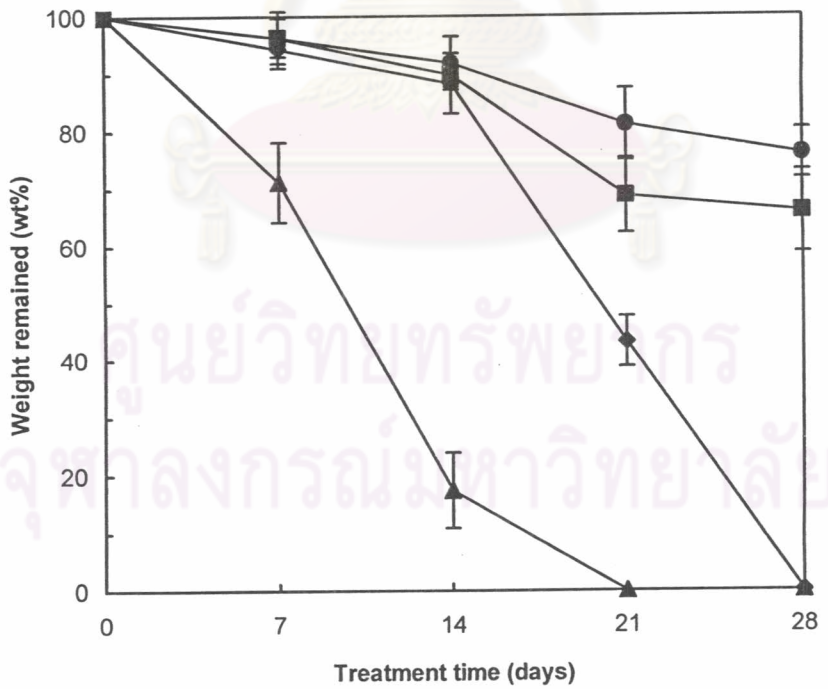

Figure 5.13 Lysozyme biodegradation of scaffolds made of collagen blended with (a) XLMW, (b) LMW, (c) MMW, and (d) HMW chitosans: (▲) 100/0, (♦) 90/10, (■) 70/30, and (●) 50/50 (ratios of collagen/chitosan).

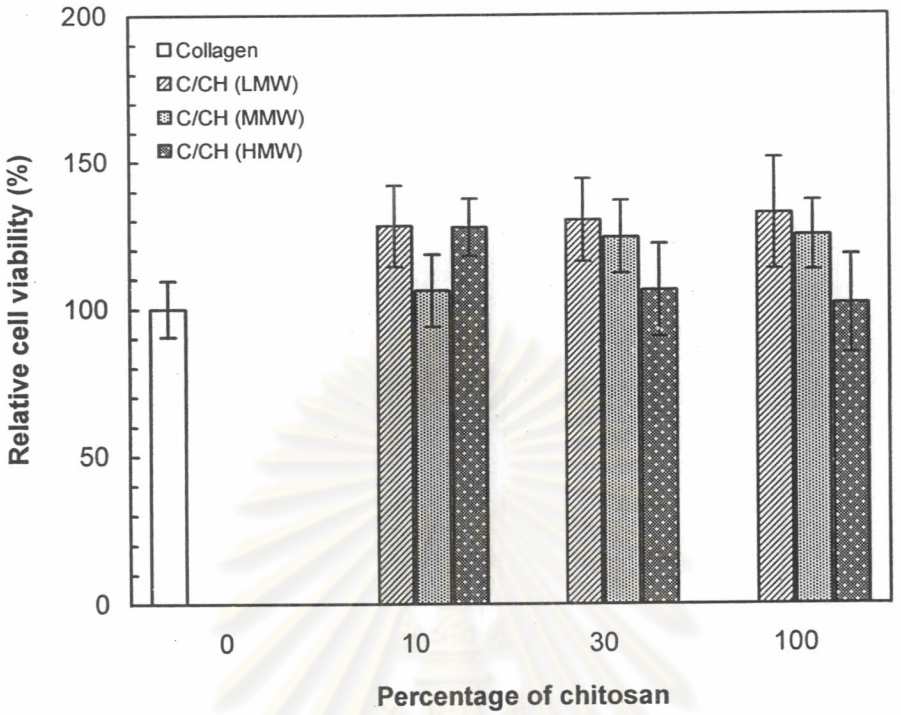

Figure 5.14 Relative cell viability (mean ± SD, n = 3, relative to pure collagen scaffold) of initial cell adhesion of L 929 on collagen/chitosan (C/CH) scaffolds with different molecular weights and blending compositions cultured in DMEM supplemented with 10% FBS.

(a)

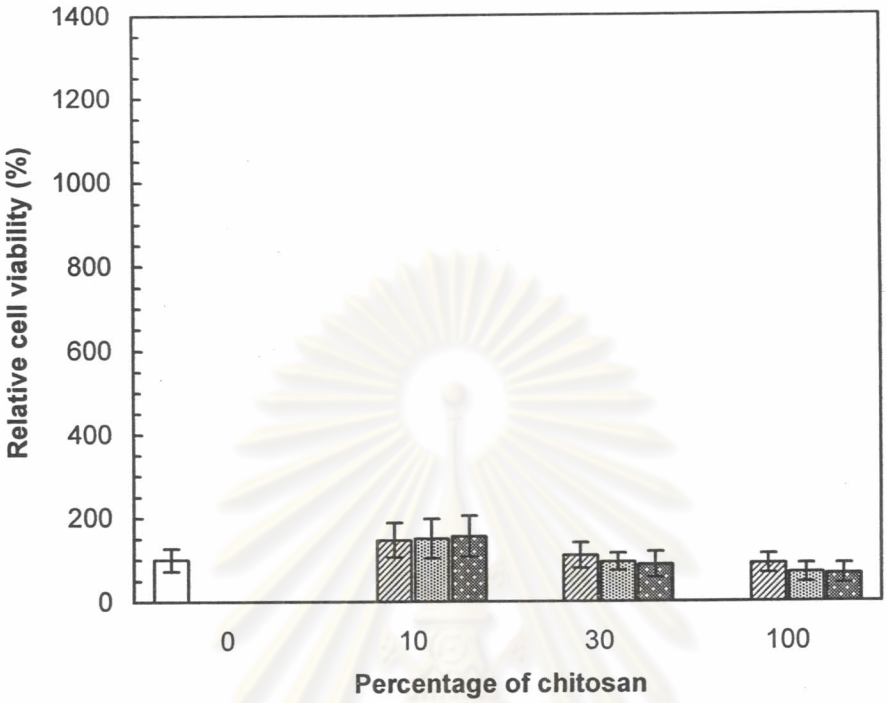

(b)

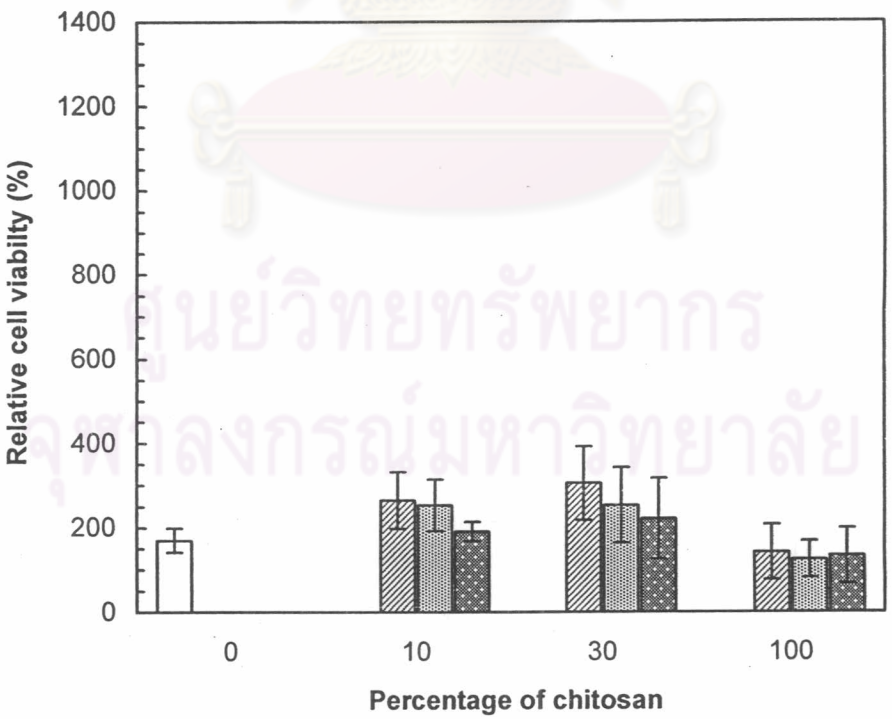

(c)

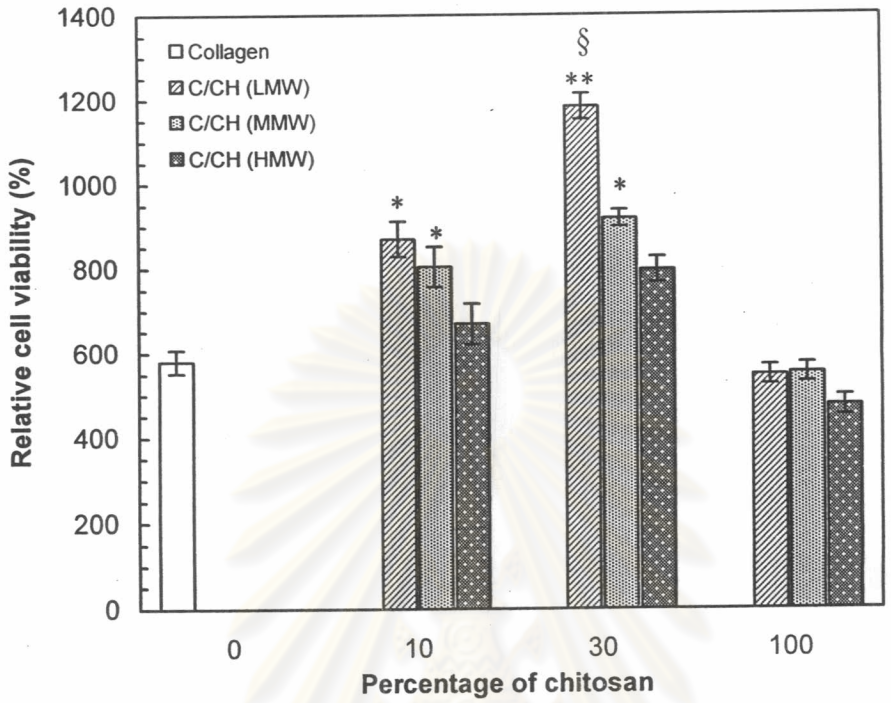

Figure 5.15 Proliferation (mean ± SD, n = 6) of L 929 on collagen/chitosan (C/CH) scaffolds cultured in DMEM supplemented with 10% FBS: (a) 5, (b) 24, and (c) 72 h after cell seeding: ** and * represented the significant difference $P<0.01$ and $P<0.05$ relative to pure collagen, respectively, and § represented the significant difference $P<0.05$ relative to all chitosans at fixed blending composition.

(a)

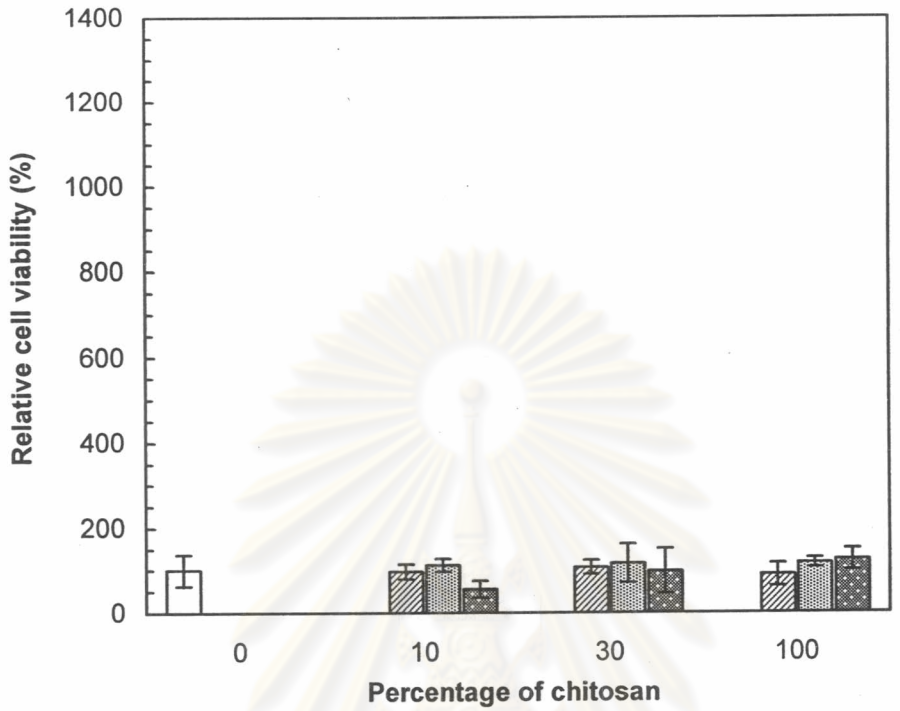

(b)

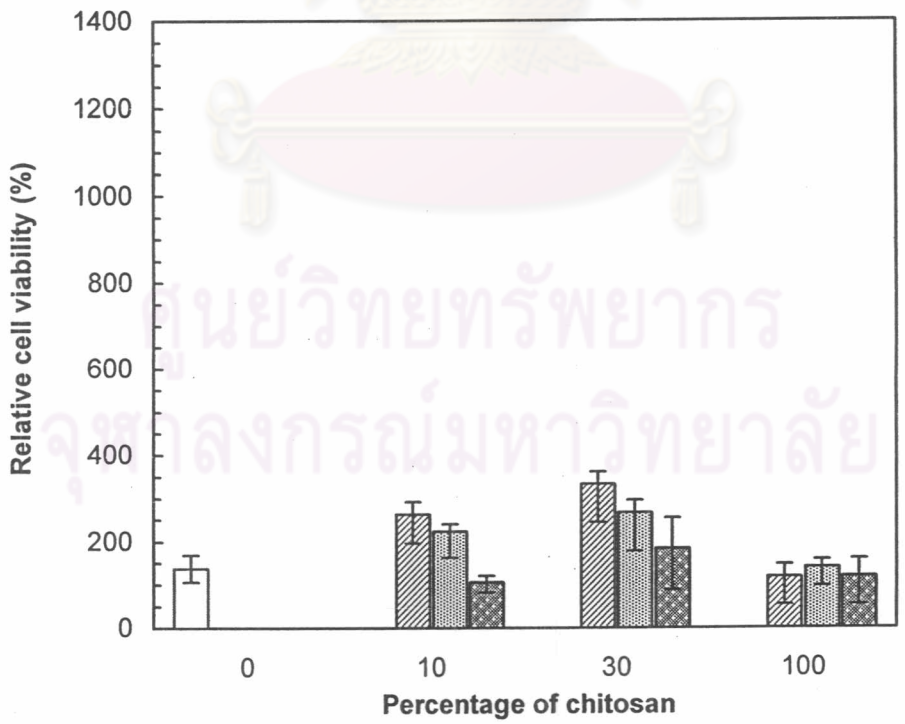

(c)

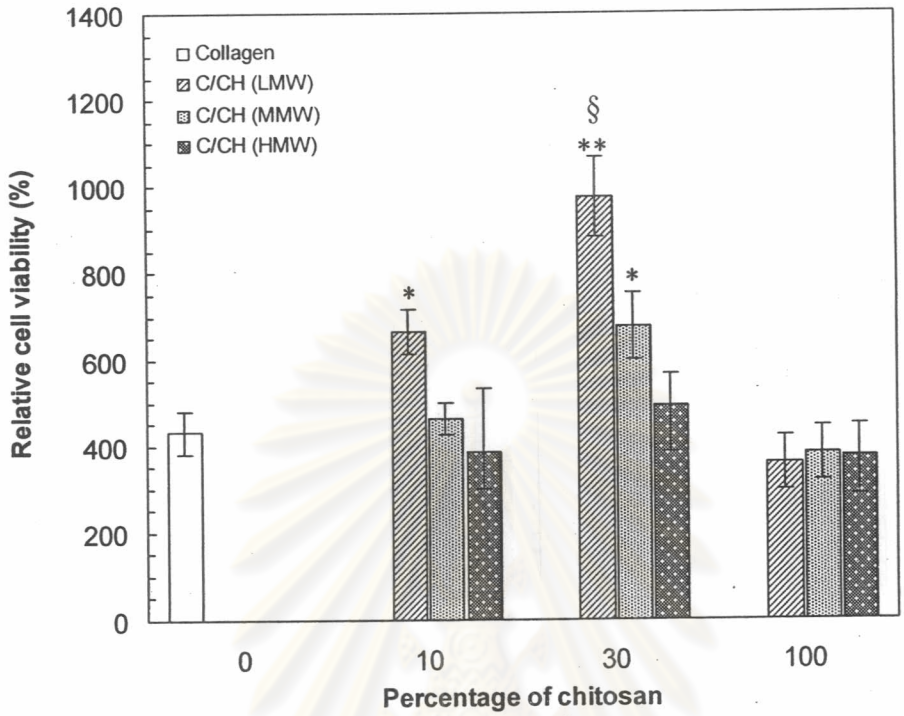

Figure 5.16 Proliferation (mean ± SD, n = 3) of L 929 on collagen/chitosan (C/CH) scaffolds cultured in serum-free DMEM: (a) 5, (b) 24, and (c) 72 h after cell seeding: ** and * represented the significant difference $P<0.01$ and $P<0.05$relative to pure collagen, respectively, and § represented the significant difference $P<0.05$ relative to all chitosans at fixed blending composition.

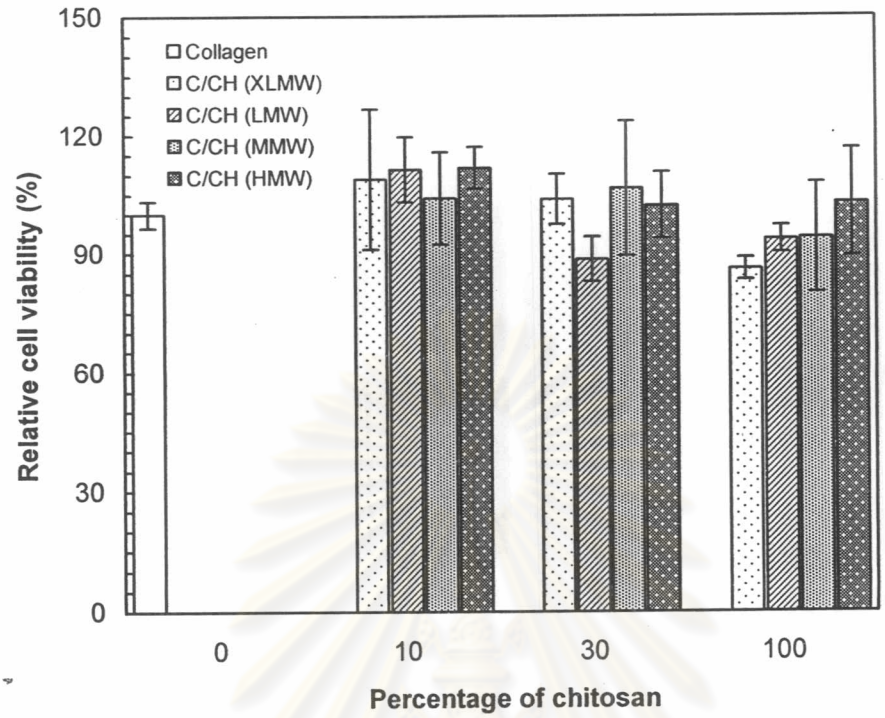

Figure 5.17 Relative cell viability (mean ± SD, n = 3, relative to pure collagen scaffold) of initial cell adhesion of Detroit 551 on collagen/chitosan (C/CH) scaffolds with different molecular weights and blending compositions cultured in DMEM supplemented with 10% FBS.

(a)

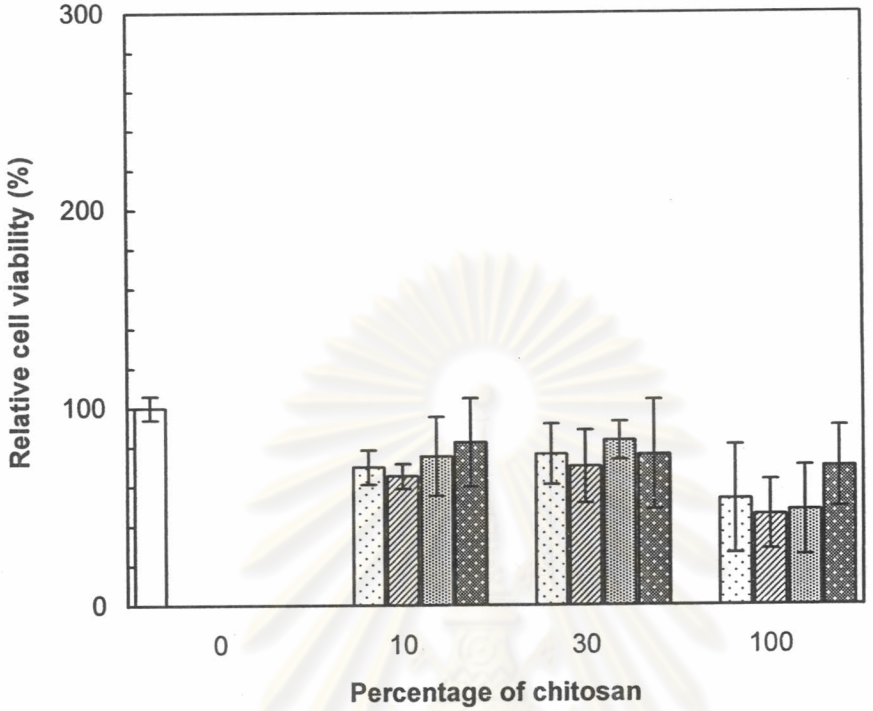

(b)

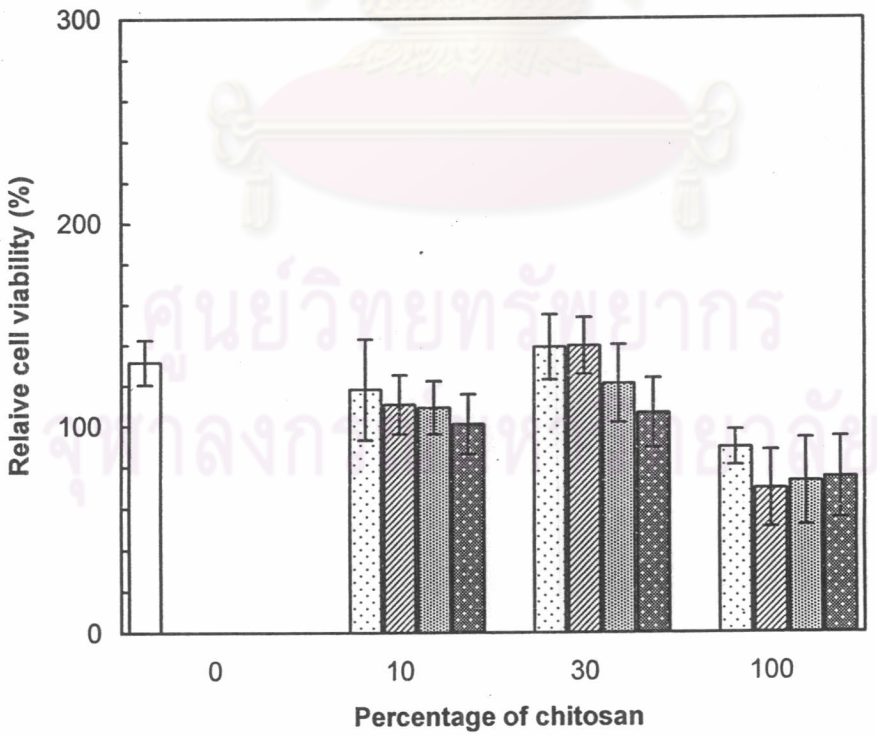

(c)

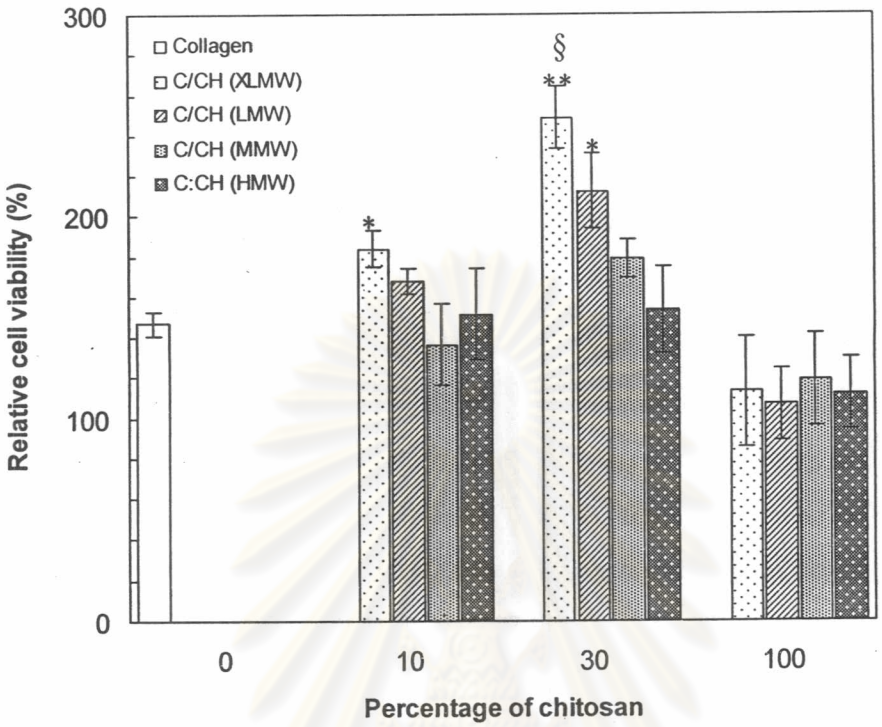

Figure 5.18 Proliferation (mean ± SD, n = 6) of Detroit 551 on collagen/chitosan (C/CH) scaffolds cultured in DMEM supplemented with 10% FBS: (a) 5, (b) 24, and (c) 72 h after cell seeding: ** and * represented the significant difference $P<0.01$and $P<0.05$ relative to pure collagen, respectively, and § represented the significant difference $P<0.05$ relative to all chitosans at fixed blending composition.

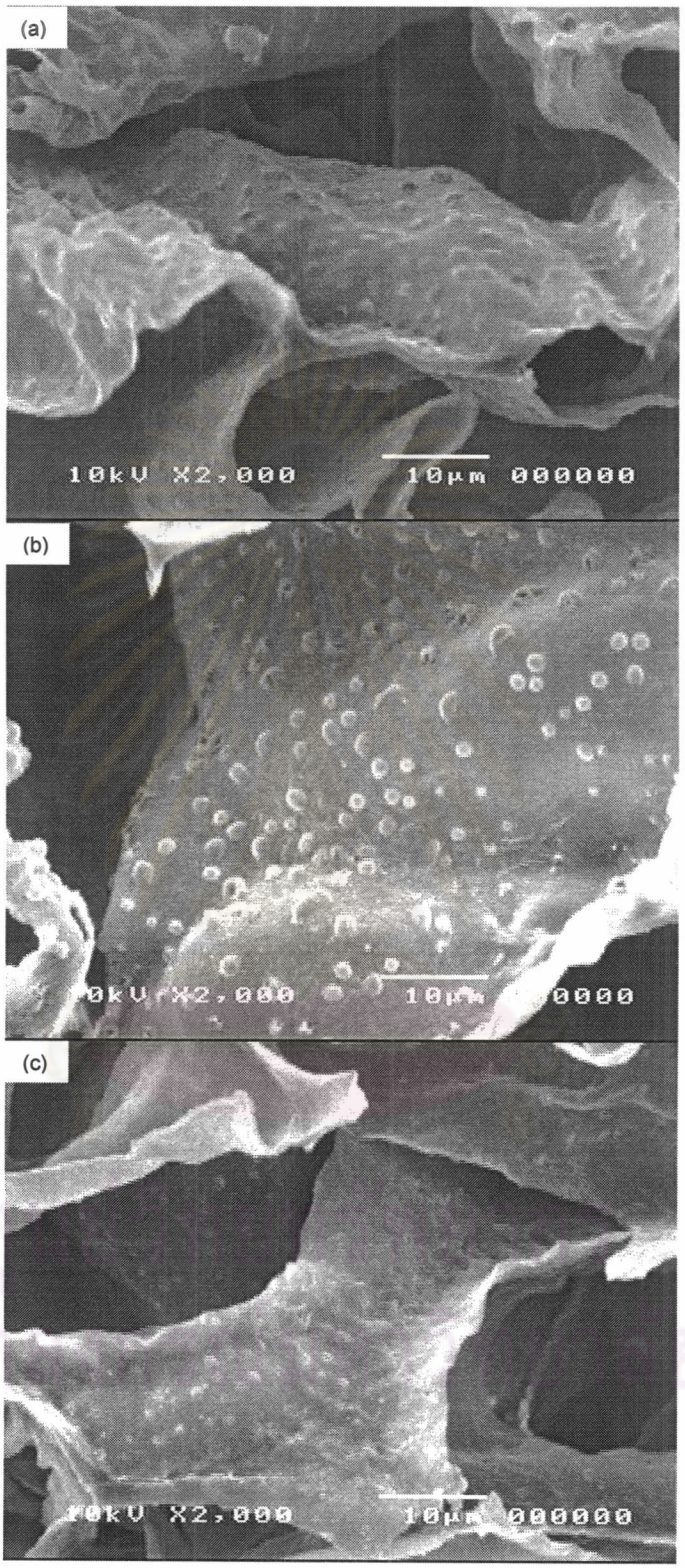

Figure 5.19 SEM micrographs of cell morphology on collagen/XLMW chitosan scaffolds: (a) 100/0, (b) 70/30, and (c) 0/100.

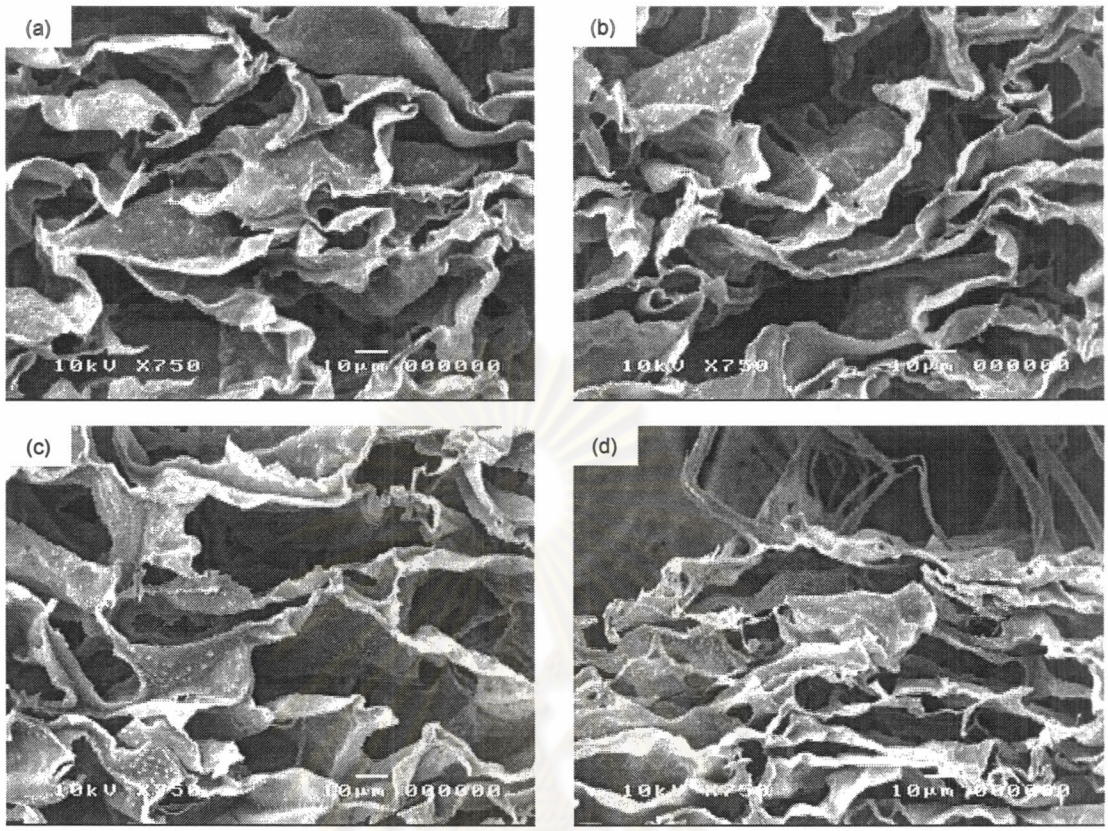

Figure 5.20 SEM micrographs of cross-sectional plane of collagen scaffolds at position (a) 1 (cell seeding side), (b) 2, (c) 3, and (d) 4 (bottom side).

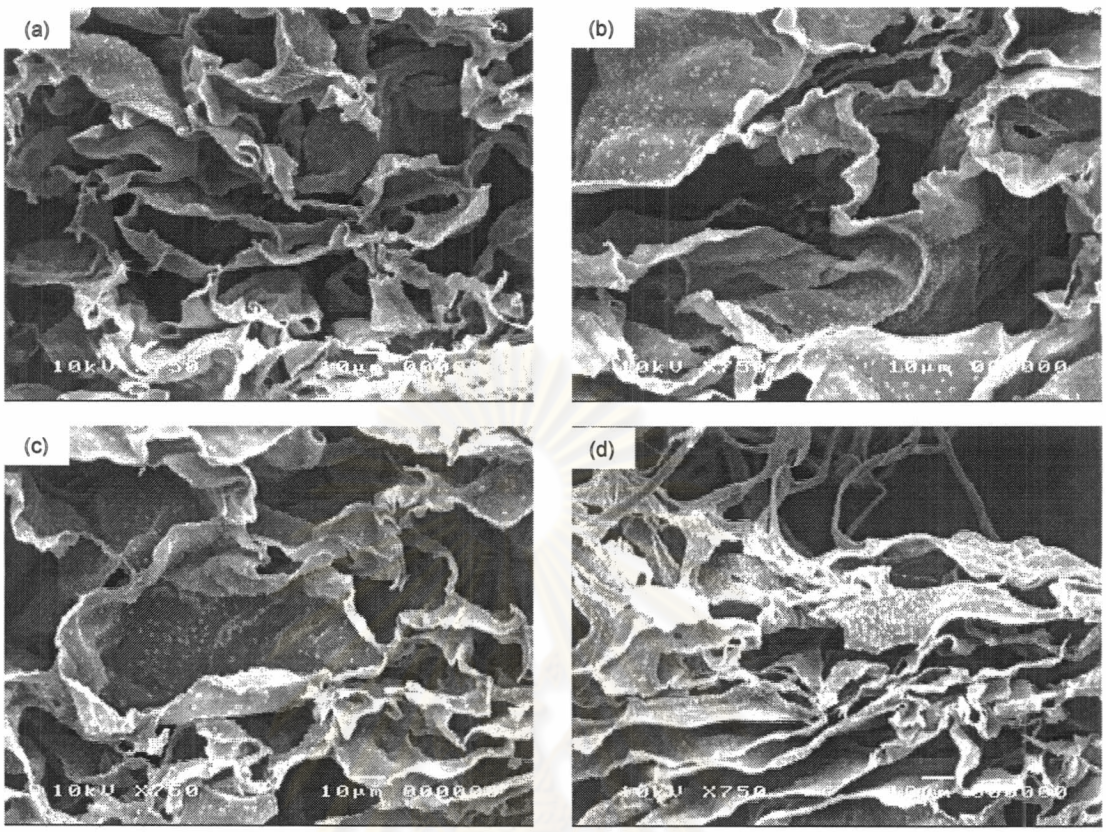

Figure 5.21 SEM micrographs of cross-sectional plane of collagen/XLMW chitosan (70/30) scaffolds at position (a) 1 (cell seeding side), (b) 2, (c) 3, and (d) 4 (bottom side).

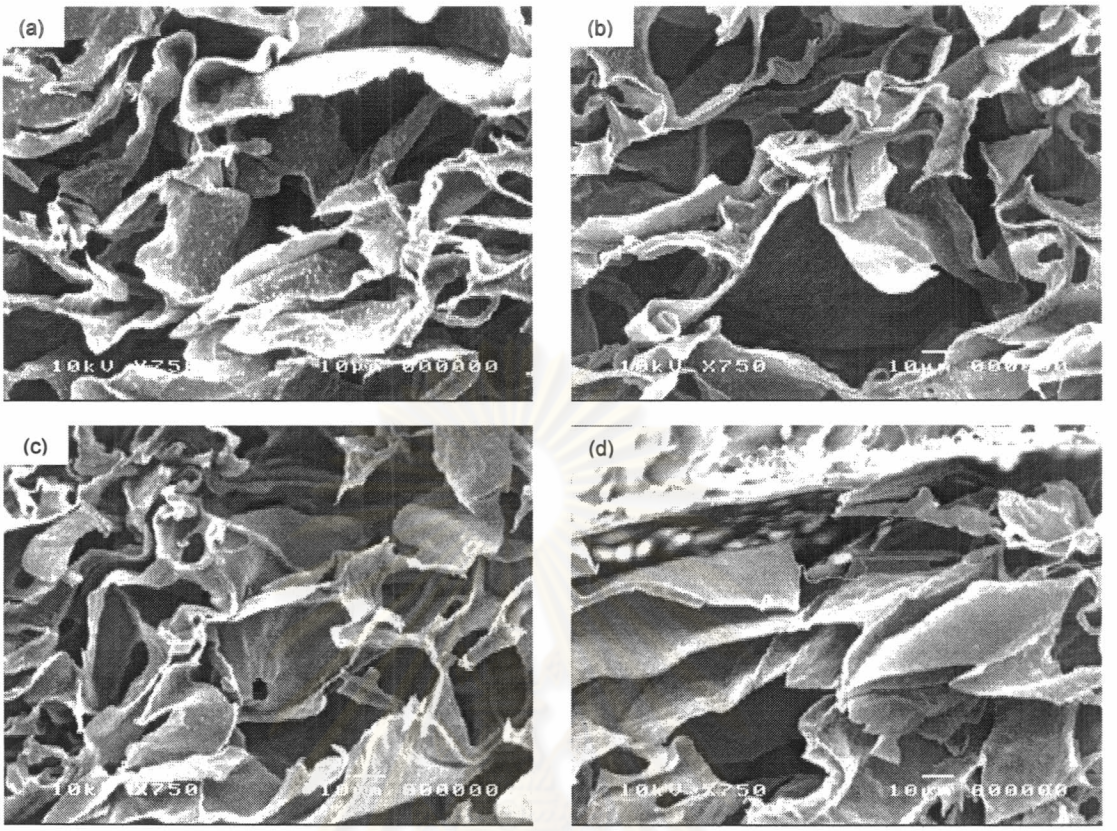

Figure 5.22 SEM micrographs of cross-sectional plane of XLMW chitosan scaffolds at position (a) 1 (cell seeding side), (b) 2, (c) 3, and (d) 4 (bottom side).

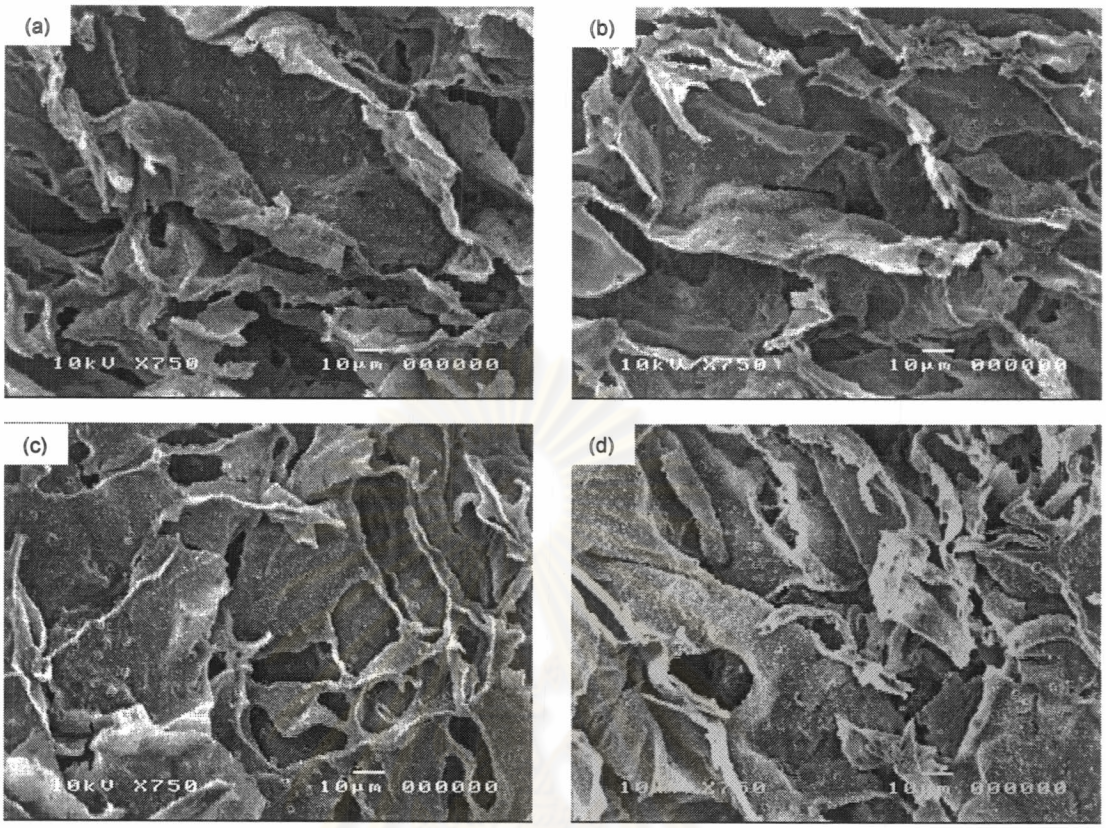

Figure 5.23 SEM micrographs of horizontal plane of collagen scaffolds at position (a) 1 (edge of scaffold), (b) 2, (c) 3, and (d) 4 (center of scaffold).

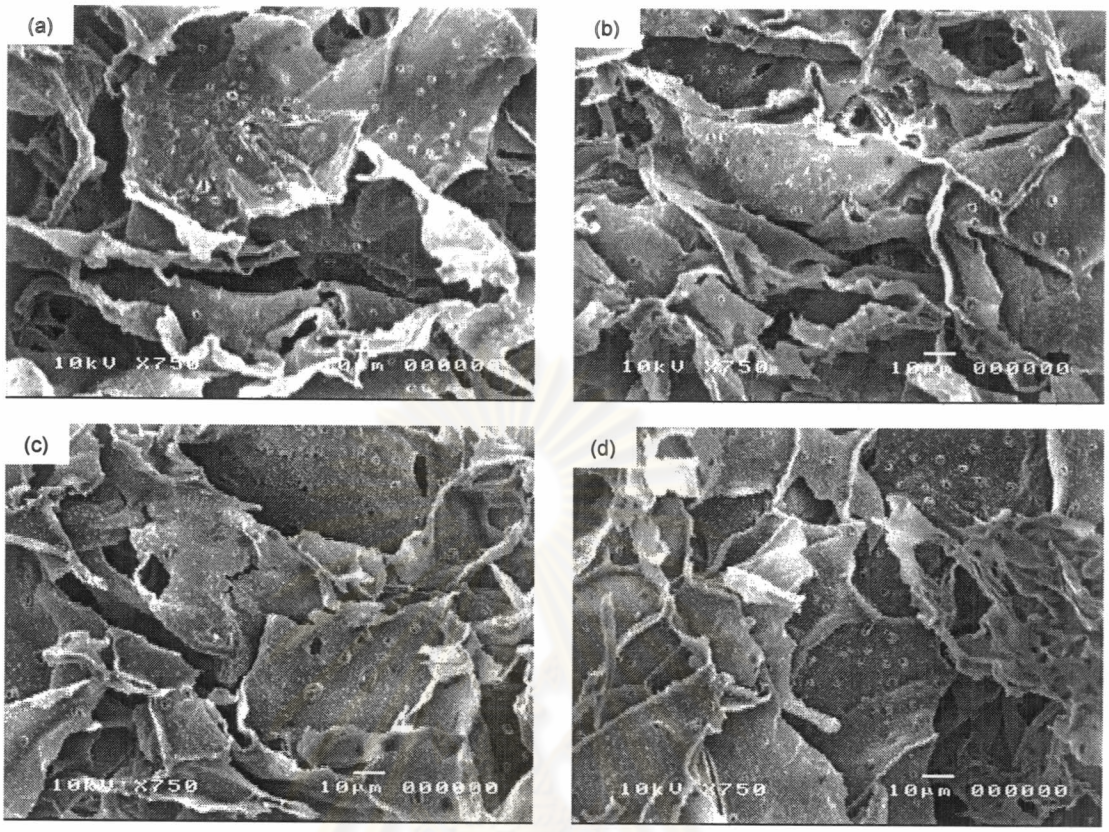

Figure 5.24 SEM micrographs of horizontal plane of collagen/XLMW chitosan (70/30) scaffolds at position (a) 1 (edge of scaffold), (b) 2, (c) 3, and (d) 4 (center of scaffold).

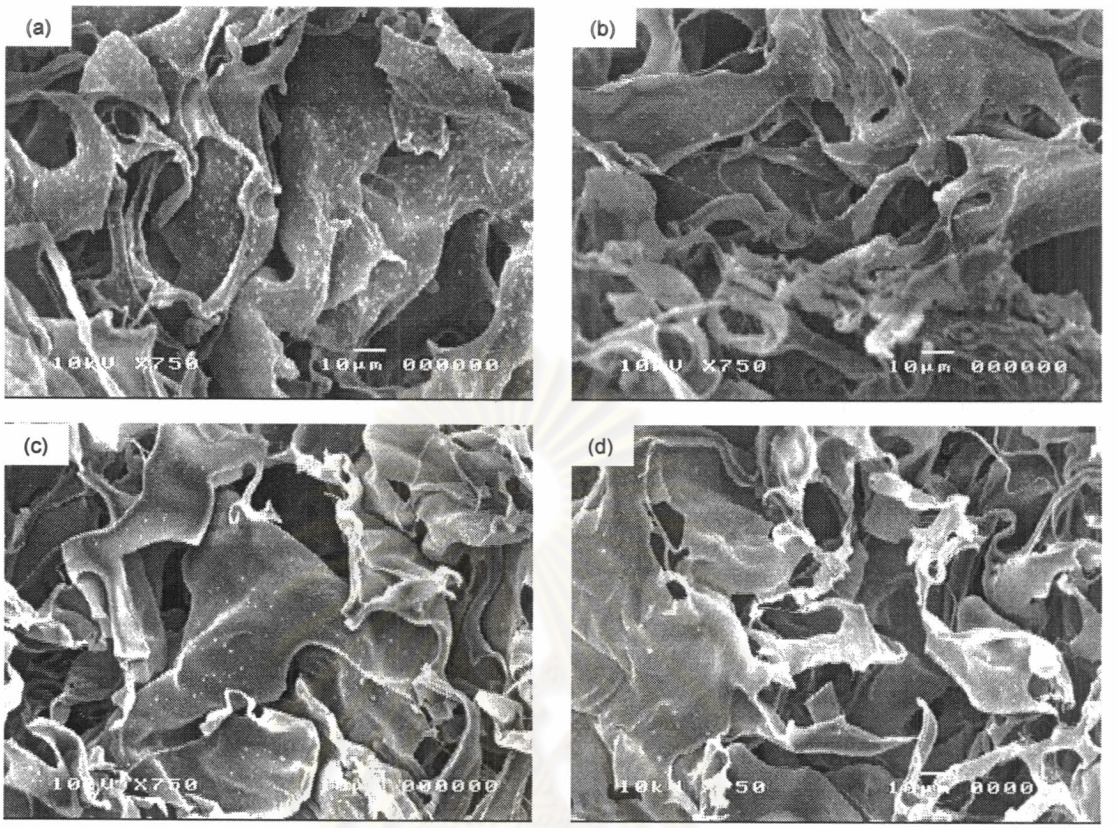

Figure 5.25 SEM micrographs of horizontal plane of XLMW chitosan scaffolds at position (a) 1 (edge of scaffold), (b) 2, (c) 3, and (d) 4 (center of scaffold).